Forschungszentrum Karlsruhe

in der Helmholtz-Gemeinschaft

Wissenschaftliche Berichte

FZKA 6776

Detailed FE-Analysis of the LCT-coil with input of displacements (Version No. 4) taken from the global model of the configuration with the TFMC

A. Grünhagen

Institut für Medizintechnik und Biophysik

Projekt Kernfusion

Forschungszentrum Karlsruhe GmbH, Karlsruhe
2002

Impressum der Print-Ausgabe:

Als Manuskript gedruckt

Forschungszentrum Karlsruhe GmbH
Postfach 3640, 76021 Karlsruhe

Mitglied der Hermann von Helmholtz-Gemeinschaft
Deutscher Forschungszentren (HGF)

ISSN 0947-8620

Detaillierte FE-Analyse der LCT-Spule mit vorgeschriebenen Verschiebungen (Version Nr. 4) aus der globalen Model-Konfiguration zusammen mit der TFMC

Zusammenfassung

Für die Entwicklung von ITER-Magneten ist das Testen einer TF-Modellspule in einer Konfiguration mit der LCT-Spule in der TOSKA-Anlage eine wichtige Vorbereitungsstufe. In diesem Versuchsaufbau muss auch die mechanische Zuverlässigkeit der LCT-Spule gewährleistet sein. Die Festigkeitsberechnungen mit dem Finite-Element-Programm ABAQUS zu dieser Spule zeigen ein unkritisches Verhalten der LCT-Struktur.

Abstract

For the development of ITER magnets, the testing of a TF model coil in the TOSKA facility is an important preliminary step. The test configuration consists of the model coil and the LCT coil. The mechanical reliability of the LCT coil has to be guaranteed in this experiment assembly. The strength calculations of this coil with the finite-element program ABAQUS show an uncritical behaviour of the LCT structure.

Contents Page

1. Introduction

The construction of the **TF** (**T**oroidal **F**ield) model coil is a major item of the R&D program for the **ITER** magnets. The main objectives of the **TF M**odel **C**oil (**TFMC**) are to demonstrate the:

- feasibility of the manufacturing processes
- reliability of the integrated system

Most of the manufacturing processes require testing before use in a full size coil, in particular the joints, the radial plates, the insertion of the conductor into the grooves, heat treatment, transfer, insertion of winding pack into casing. Of course, separate tests will be performed for each item, but the feasibility of the whole concept will only be demonstrated by manufacturing a model including all different features of the coil.

The test of an integrated system is the only way to fully qualify the different techniques used during the manufacture. The extensive test program must be representative concerning the constraints which occur in the real device. Furthermore, the test should be able to evaluate the safety margins of the parameters investigated.

In the test configuration the TFMC is positioned adjacent to the LCT coil under an angle of 4.5 degrees (figures 1 and 2) in the TOSKA facility at the Forschungszentrum Karlsruhe.

2. Finite Element Analysis

2.1 Objective

The assembly of the test configuration consists of the TFMC (winding, casing, and support structure), intercoil structure, and the LCT coil (figures 1 and 2). The magnetic field is computed with EFFI /1/ for a current I=70 kA of the TFMC winding and I=16 kA for the LCT winding. The D-shaped LCT coil produces the magnetic background field for the test with the TFMC. The coil systems in the TOSKA reference coordinate system are subject to an attraction force (out-of-plane) of F_y=72.3 MN and an in-plane force of F_x=12.8 MN. The intercoil structure connects both coils and provides for the transfer of the in-plane and out-of-plane forces. The attraction forces are transmitted by a set of five horizontal plates inserted between the steel belts of the LCT-coil. Three upper and three lower belts of the original twelve steel belts are removed. From the remaining outer-most lower and upper belt, one inner half belt was removed, too for increasing the thickness of the two outer-most horizontal plates. Over the whole width, two pads positioned at the top and at the bottom of the LCT casing are also utilised for the transmission of these forces. The in-plane forces are transferred by two hooks situated at the outer corners of the LCT casing. Furthermore, the five horizontal plates have hooks resting on the LCT casing side plate. The hooks will also be used for the transmission of the in-plane forces.

The behaviour of the LCT coil in this assembly is of great interest. The calculations of the deformations and the stresses are performed by the **F**inite **E**lement **M**ethod (**FEM**) with the program system ABAQUS /2/.

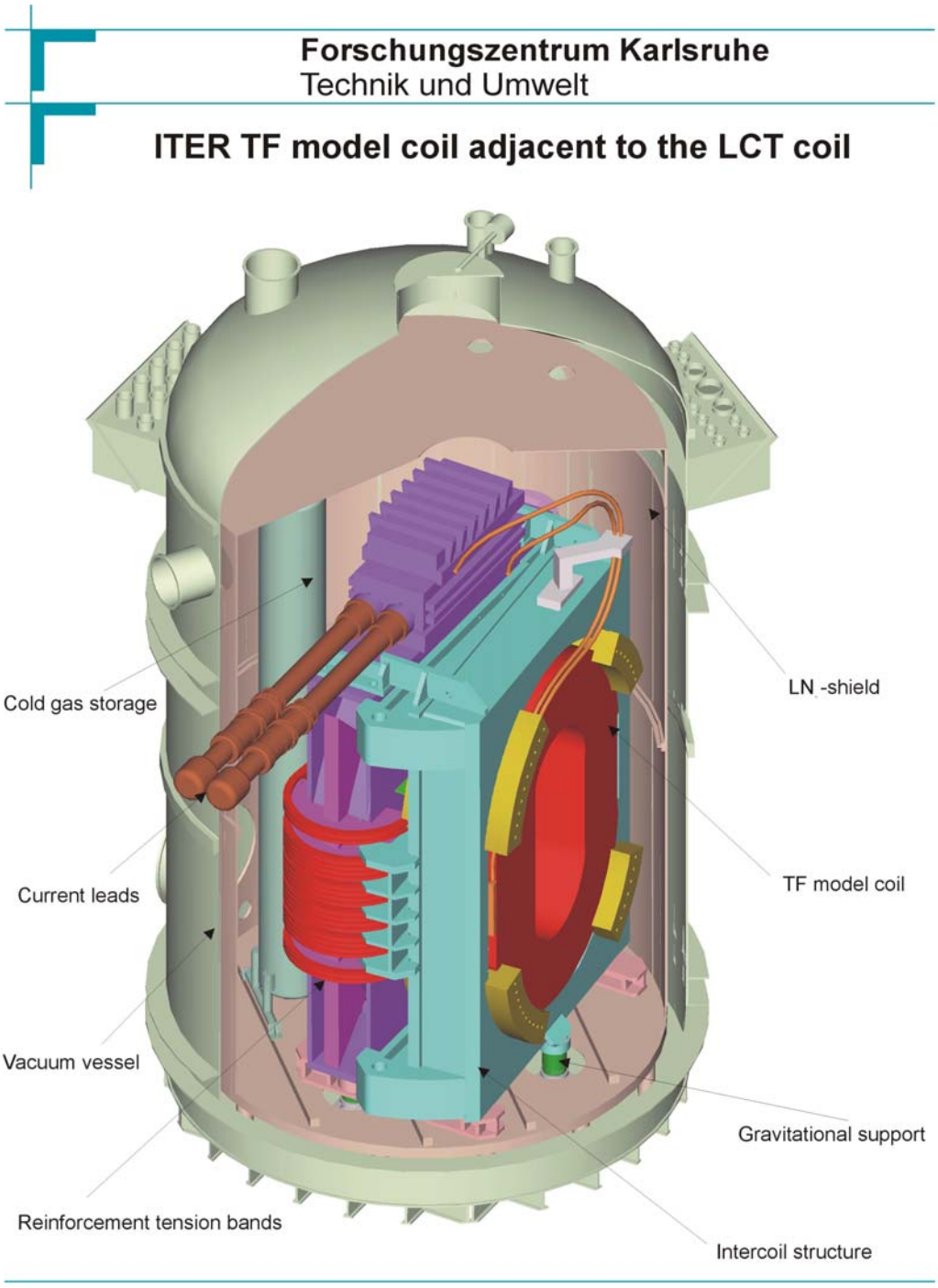

Figure 1 - LCT-ITER TF model coil configuration in TOSKA

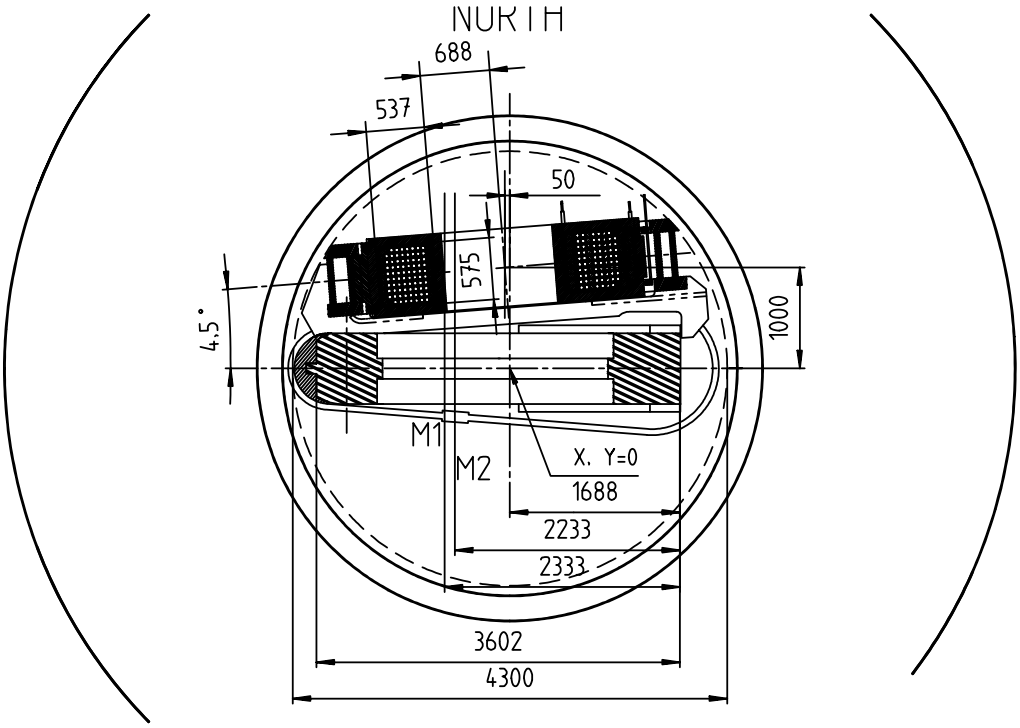

Figure 2 - Top view of the LCT-ITER TF model coil configuration in TOSKA

2.2 Model Description

For structure analyses of the LCT coil, an existing FE model /3/ was used. A complete FE model with this detailed LCT model has not been developed. Figure 3 shows the FE model of the LCT-coil.

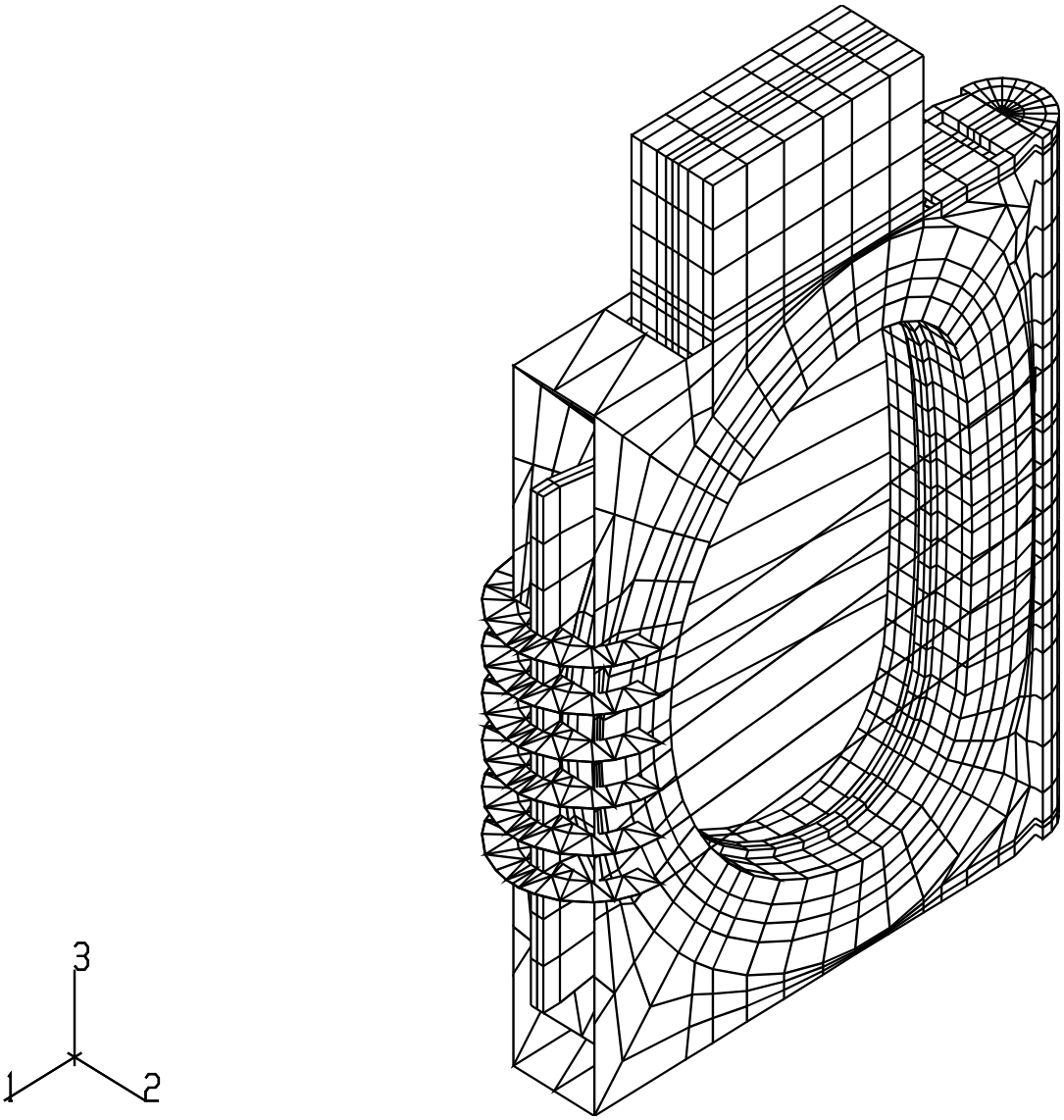

Figure 3 – FE model of the LCT coil

The choice of elements and the material behaviour of the LCT coil are described in detail in the report /3/. The model was meshed with 9546 elements, 13501 nodes, and 40044 degrees of freedom. Figure 3a represents the coordinate-sytems of the model; 123- respectively xyz-direction is the global rectangular coordinate system and rzφ-direction is the local cylindrical coordinate system of the winding.

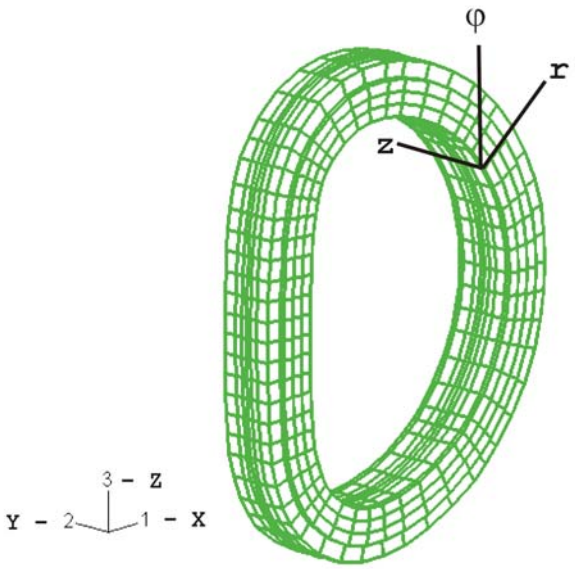

Figure 3a – Coordinate-systems of the LCT-coil

The link between the intercoil structure and the LCT casing was simulated with the following boundary conditions shown in figure 4:

- Four nodes (z_1 ,z_2, z_3, and z_4) at the bottom of the LCT casing are fixed in z-direction
- All other marked nodes simulate the intercoil structure. All these nodes are subject to a prescribed displacement (**Table 1**)/5/, which simulates the deformation between the LCT and ITER model coil.
  The five horizontal lines show the z-positions of the horizontal plates of the intercoil structure.

POINT	X-DISPLACEMENT	Y-DISPLACEMENT
9341		0.41873E+01
9348		0.41289E+01
9375		0.65996E+01
9414		0.41860E+01
9468		0.45340E+01
9496		0.67231E+01
9569		0.44258E+00
9576		0.25004E+00
9642		0.22476E-02
9696		0.10568E+01
9717		0.14230E+01
9753		-0.19846E+00
9864	-0.16822E+01	
9996	-0.31725E+00	
15281		0.26127E+01
15459		0.30781E+01
15640		0.33448E+01
15821		0.35363E+01
16003		0.35991E+01
19044		0.61879E+01
19051		0.61233E+01
19076		0.23615E+00
19110		0.62837E+01
19166		0.62239E+00
19468		0.46378E+01
19469		0.50303E+01
19470		0.41304E+01
19471		-0.85983E-01
19472		-0.54934E-01
19473		-0.20019E+00
19507	-0.15160E+01	
19549		0.57888E+01
19552		0.57312E+01
19584	-0.18894E+01	
19626		0.66439E+01
19629		0.66091E+01
19659	-0.19809E+01	
19699		0.78035E+01
19702		0.78830E+01
19731	-0.21096E+01	
19771		0.75873E+01
19774		0.76086E+01
19805	-0.20974E+01	
19847		0.71856E+01
19850		0.71806E+01

Table 1

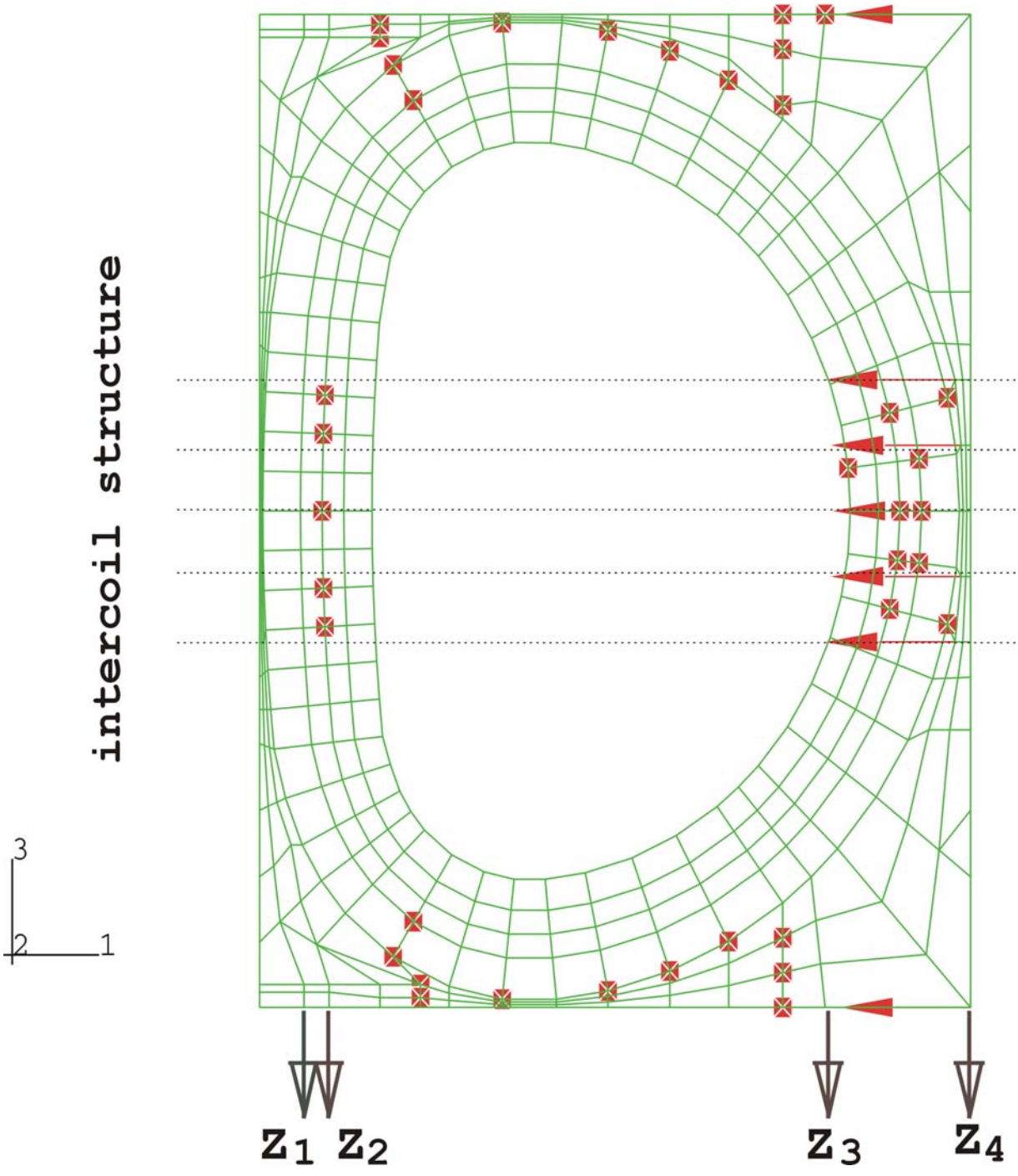

Figure 4 - Boundary conditions in x-, y- and z-direction of the LCT coil

The material behaviour of the **LCT casing** is assumed to be isotropic.

Young's modulus $E = 2.1E+05$ MPa
Poisson's ratio $\nu = 0.3$
0.2 strength $\sigma_{0.2} = 1050$ MPa (4^{o} K)

The material behaviour of the **LCT winding** is assumed to be orthotropic (rzφ-direction is the local cylindrical coordinate system in figure 3a) and all material data are summarised in Table 2.

critical shear stress τ = 50 MPa

winding radius				
	Young's modulus	R1 front of winding	R2 transition zone	R3 back of winding
radial	E_r [GPa]	10.0	14.9	2.7
azimuthal	E_φ [GPa]	120.0	120.0	120.0
axial	E_z [GPa]	53.0	53.0	53.0
	Poisson number			
	$\nu_{\varphi r}$	0.298	0.298	0.298
	$\nu_{z\varphi}$	0.126	0.126	0.126
	ν_{rz}	0.145	0.145	0.145
	G modulus			
	$G_{r\varphi}$ [GPa]	21.0	21.0	21.0
	$G_{z\varphi}$ [GPa]	26.0	26.0	26.0
	G_{rz} [GPa]	10.0	10.0	10.0

Table 2

2.3 Results

The presentations of the results are plotted with ABAQUS-Post /4/ and ABAQUS-Viewer /6/. In Fig. 5 the distributions of the von Mises stress are illustrated as discrete filled colour levels in a detail view of the structure. Each coloured contour corresponds to a range bounded by the values indicated on the similarly coloured band within the legend. It is difficult to show the stress distribution on the surface of the LCT casing, because there is not such a great variety of the values. On an average, the stresses amount to approximately **σ_v=70 MPa**.

casing	**von Mises stress [MPa] σ_v**
maximum	**320.5**

Table 3 - Casing

$\sigma_{0.2}$ = 1050 MPa (4^o K)

The maximum equivalent von Mises stress (Table 3) has the value **σ_v=320.5 MPa** and is about 70% lower than the strength $\sigma_{0.2}$.

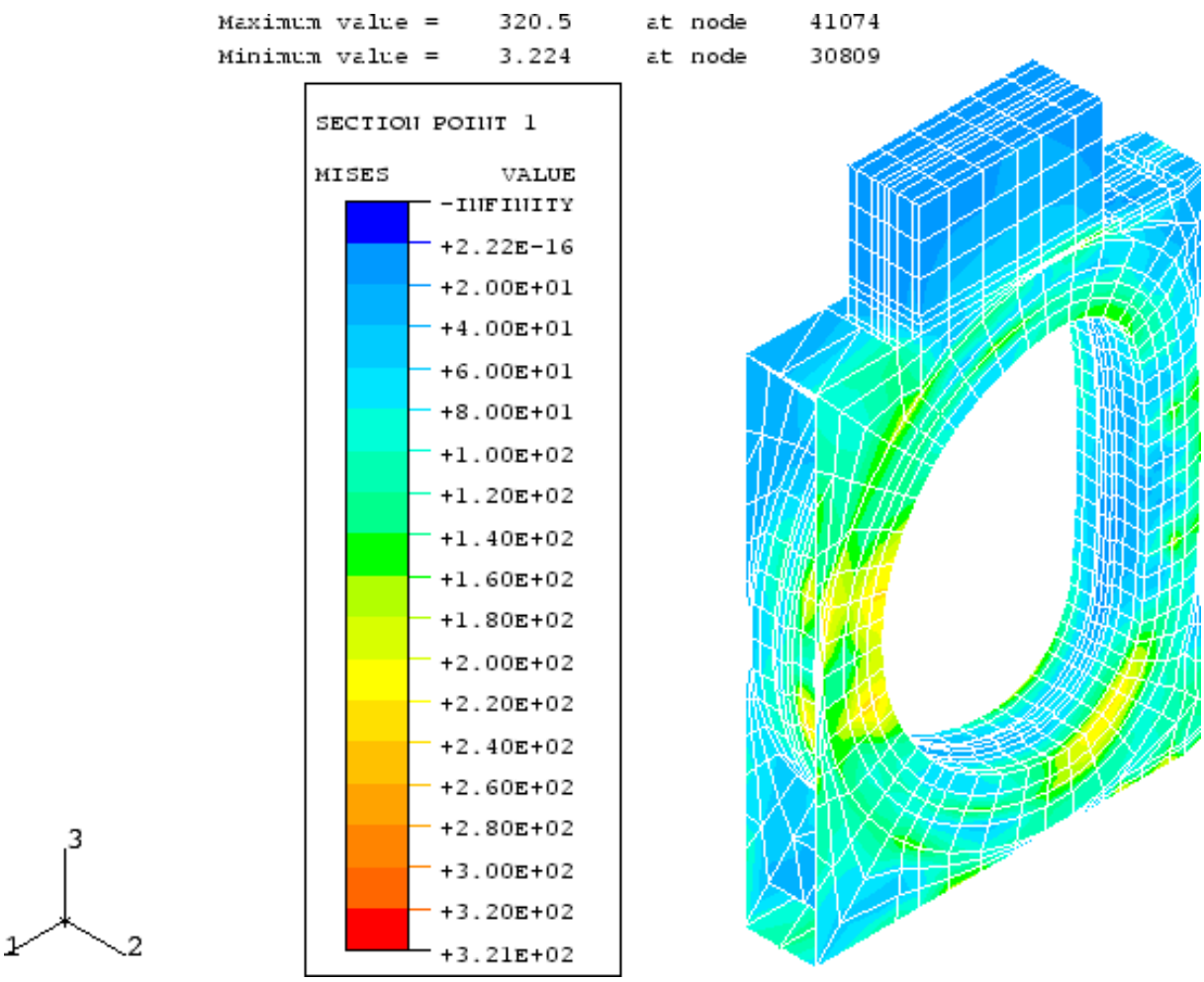

Figure 5 - Contour plot of von Mises stresses in a detail view of the LCT-casing

The maximum shear stresses of the LCT winding (rzφ-direction is the local cylindrical coordinate system in figure 3a) are summarised in tables 4 and 5.

winding	normal stress [MPa]		
	σ_r	σ_z	σ_φ
maximum	-0.657	+24.60	+193.0
minimum	-37.92	-145.8	-32.08

Table 4 – LCT winding

winding	shear stress [MPa]		
	τ_{rz}	$\tau_{\varphi z}$	$\tau_{r\varphi}$
maximum	+36.81	+20.08	+23.57
minimum	- 9.76	-21.24	-25.60

Table 5 – LCT winding

critical shear stress τ = 50 MPa

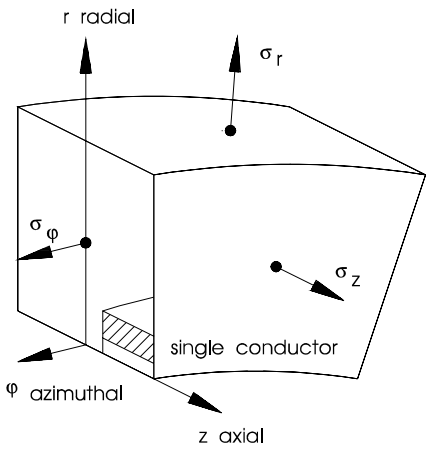

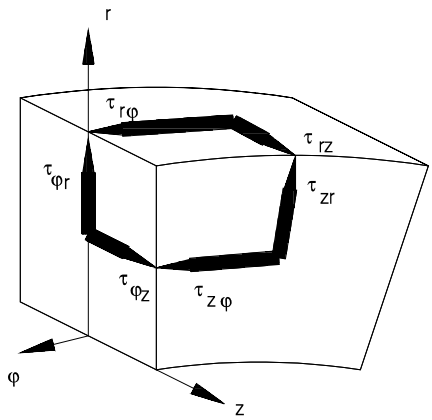

The maximum shear stress of the winding $\mathbf{|\tau_{rz}|=36.81\ MPa}$ (table 5) is 26% lower the critical shear stress $\mathbf{\tau=50\ MPa}$. The regions with the maximum stresses are at the outer edge of the winding (figure 6). The other shear stresses are also far away from the critical shear stress. They are about 50% smaller than the limit value. Figures 7 and 8 show the stress distributions $\tau_{\varphi z}$ and $\tau_{r\varphi}$. In figures 12, 13, 14, 15, 16 and 17 the shear stresses τ_{rz}, $\tau_{\varphi z}$, and $\tau_{r\varphi}$ of the LCT winding are plotted over the azimuth angle of the winding. The azimuthal graduation of the structure is given in figure 9. The maximum shear stresses τ_{rz} appear on the position lines W79, which can be taken from figures 10 and 11. Both peaks of the shear stresses τ_{rz} are situated about symmetrically at opposite positions of 69.7^{o} **(36.81 MPa)** and 298.7^{o} **(32.00 MPa).** They are located above the uppermost and below the lowermost horizontal plate of the intercoil structure. The peaks are very small and decrease by about **10 MPa** at a distance of 1 or 2 element lengths off the peak position. The shear stresses τ then are smaller than the limit value about a factor of **1.86**.

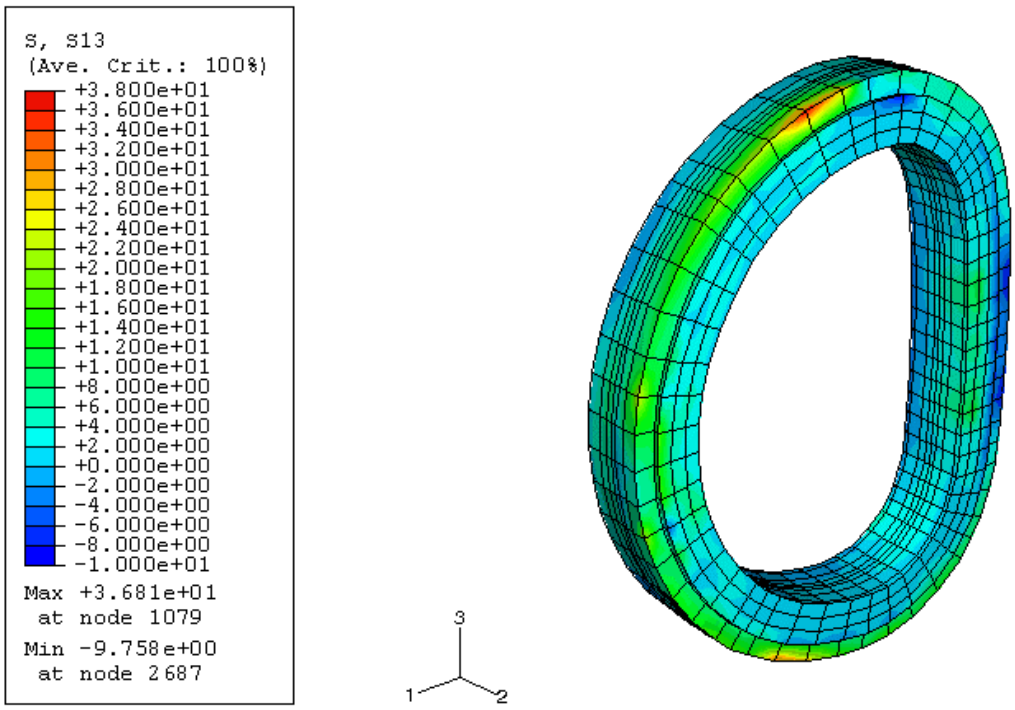

Figure 6 - Contour plot of shear stresses τ_{rz} of the LCT winding

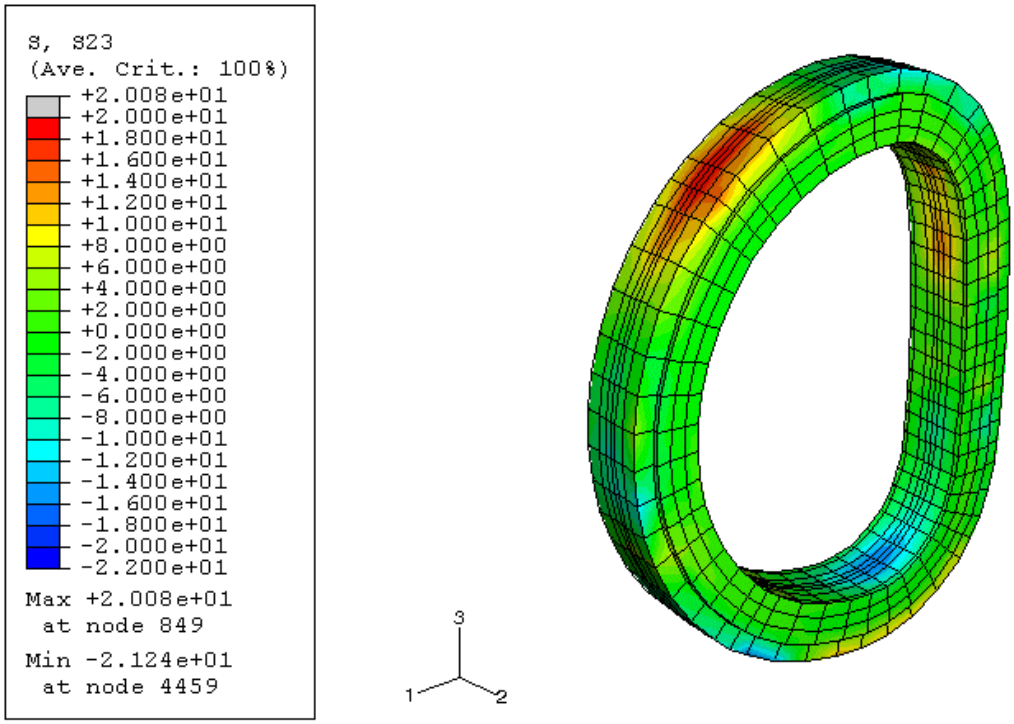

Figure 7 - Contour plot of shear stresses $\tau_{\varphi z}$ of the LCT winding

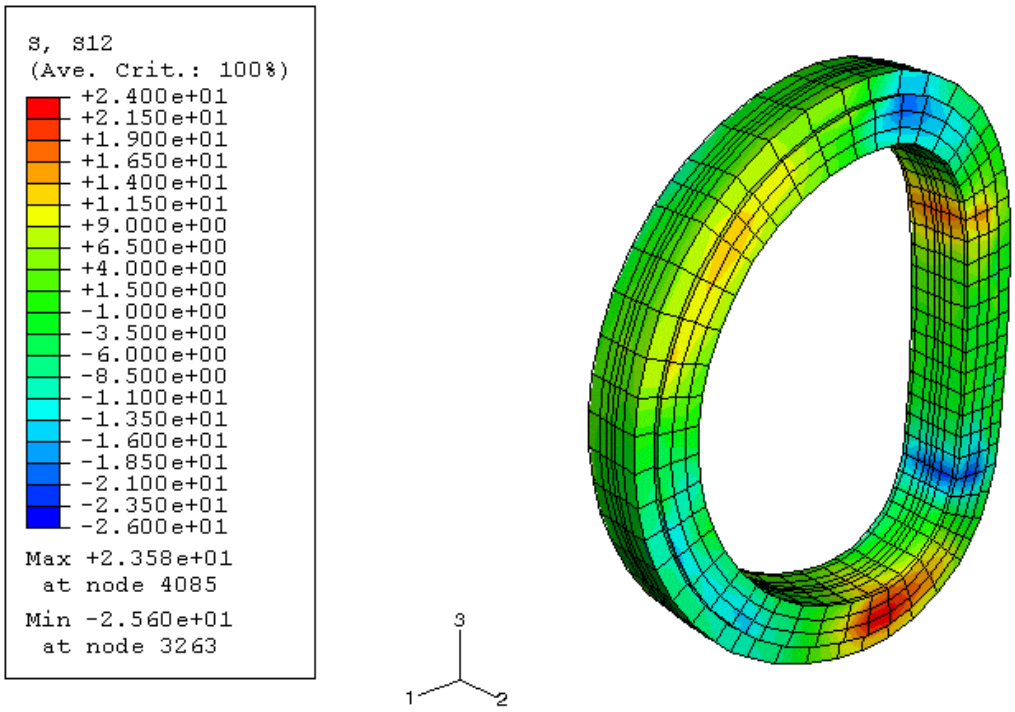

Figure 8 - Contour plot of shear stresses $\tau_{r\varphi}$ of the LCT winding

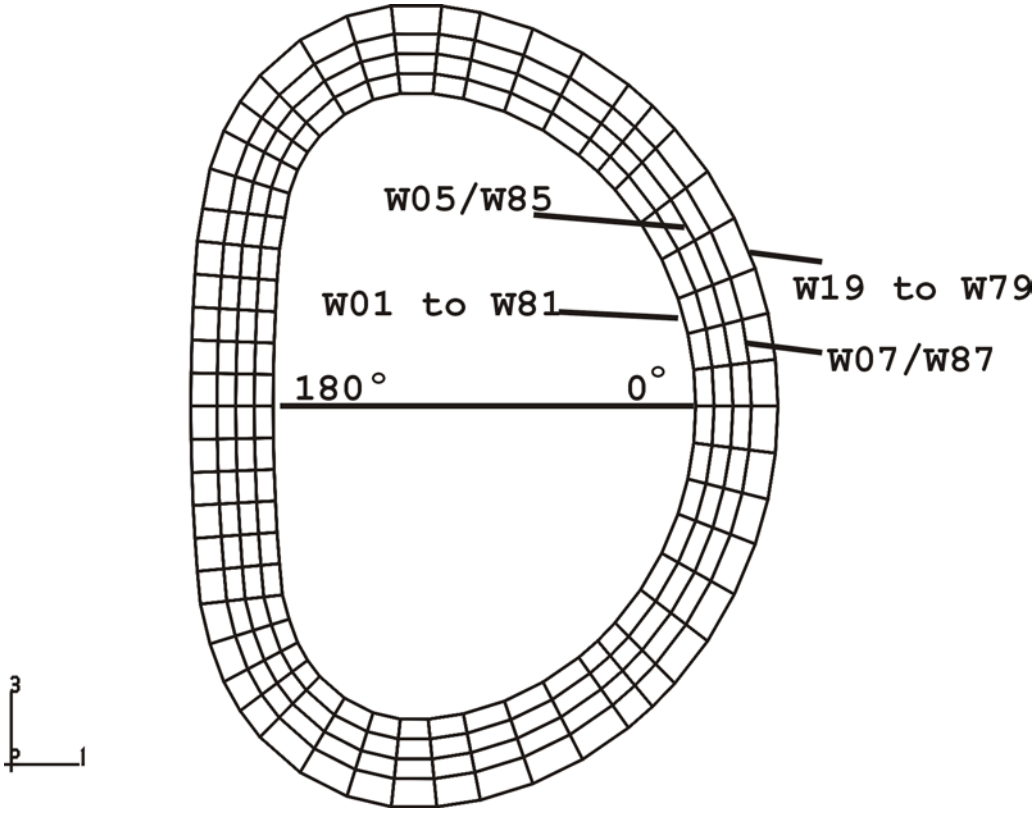

Figure 9 - Azimuthal graduation of the LCT winding and description of the position lines

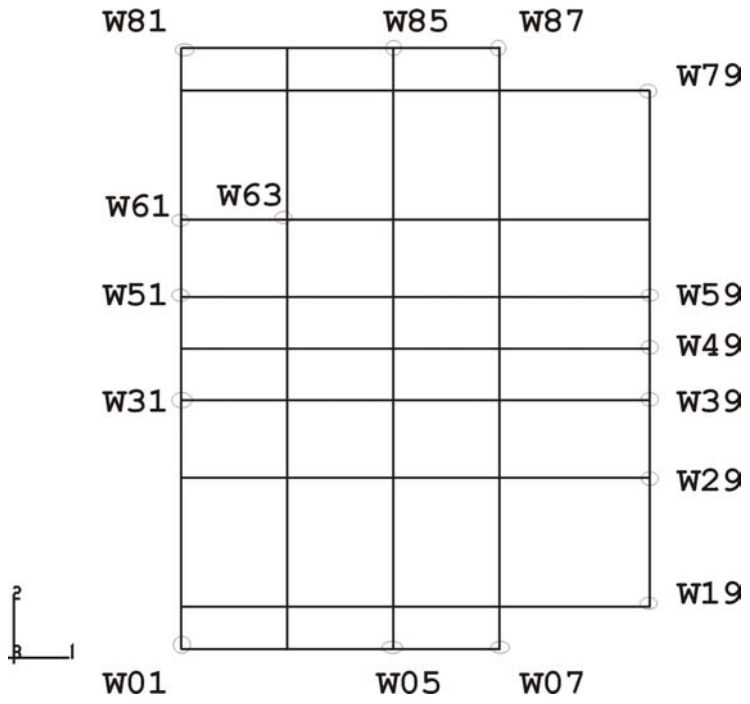

Figure 10 - Cross section of the LCT winding with a description of the position lines

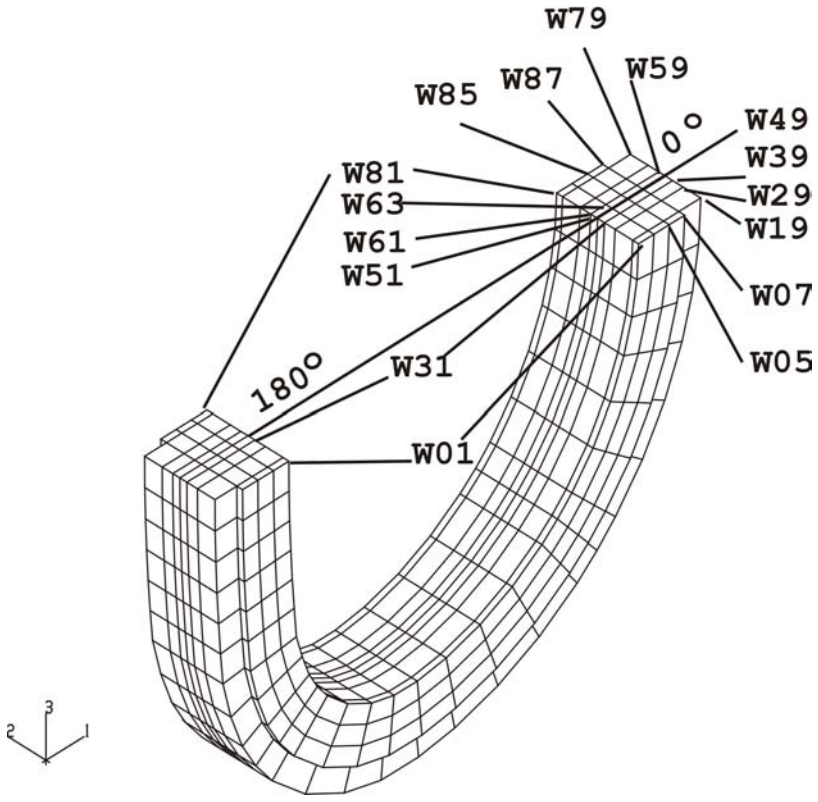

Figure 11 - Lower half of the LCT winding with a description of the position lines

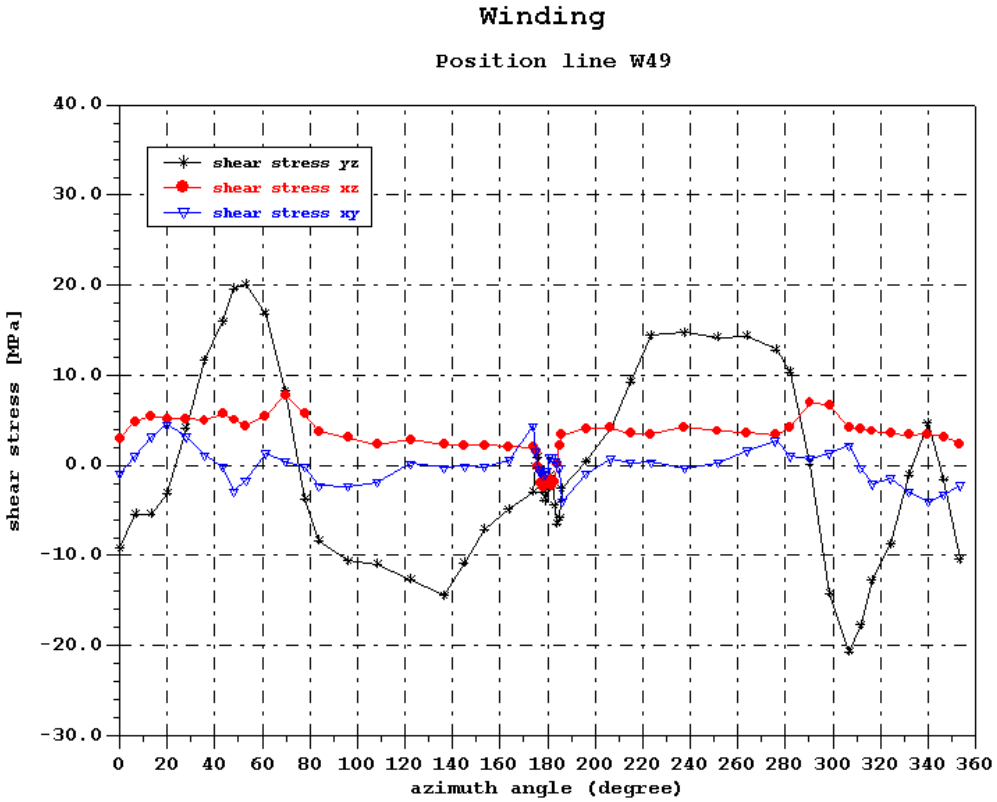

Legend: shear stress xz - τ_{rz}
shear stress yz - $\tau_{\varphi z}$
shear stress xy - $\tau_{r\varphi}$

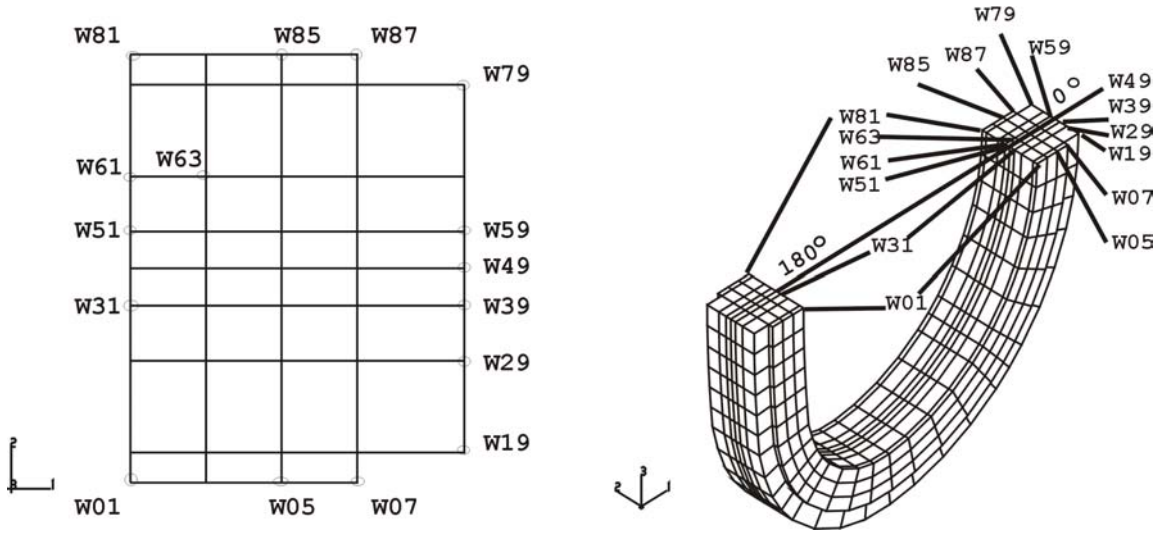

Figure 12 - Shear stresses of the LCT winding over the azimuth angle on the position line W49

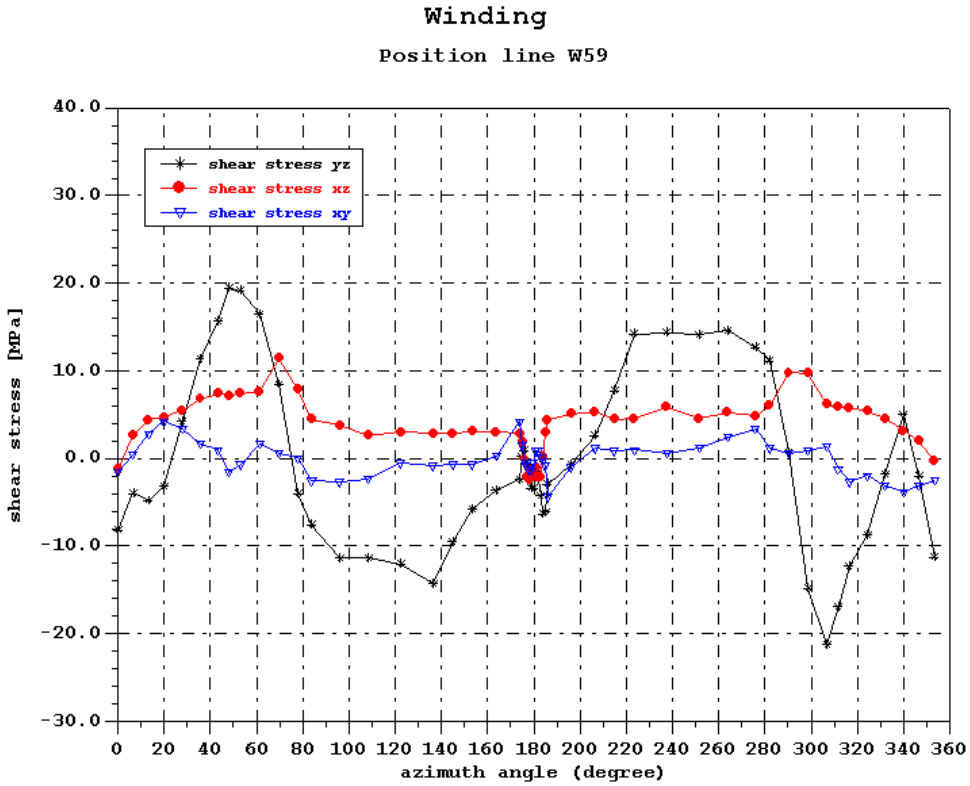

Legend: shear stress xz - τ_{rz}
shear stress yz - $\tau_{\varphi z}$
shear stress xy - $\tau_{r\varphi}$

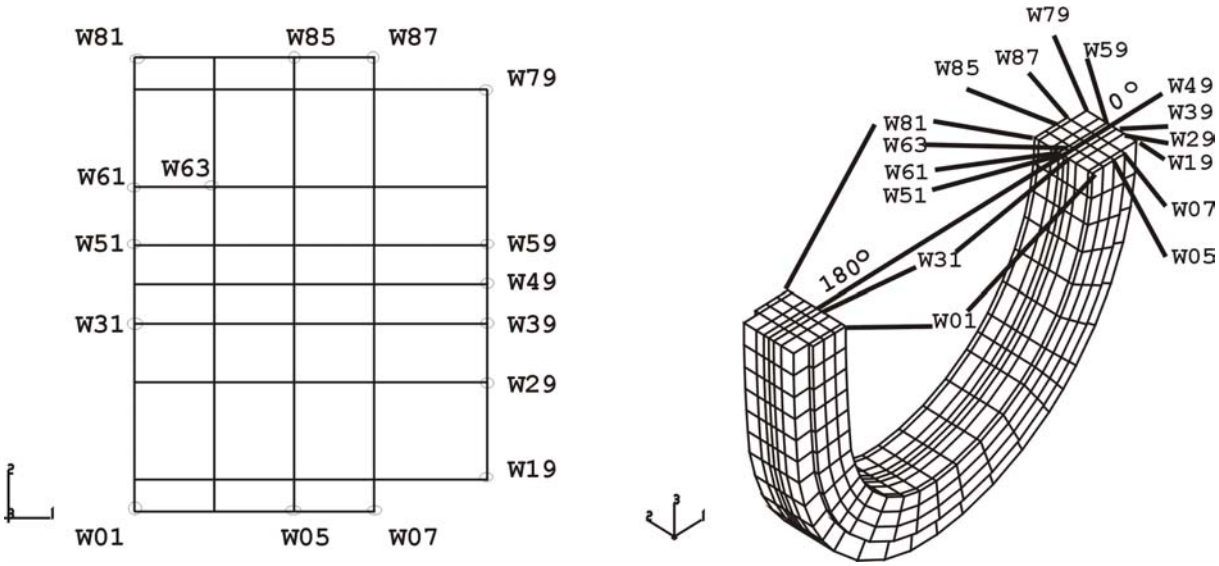

Figure 13 - Shear stresses of the LCT winding over the azimuth angle on the position line W59

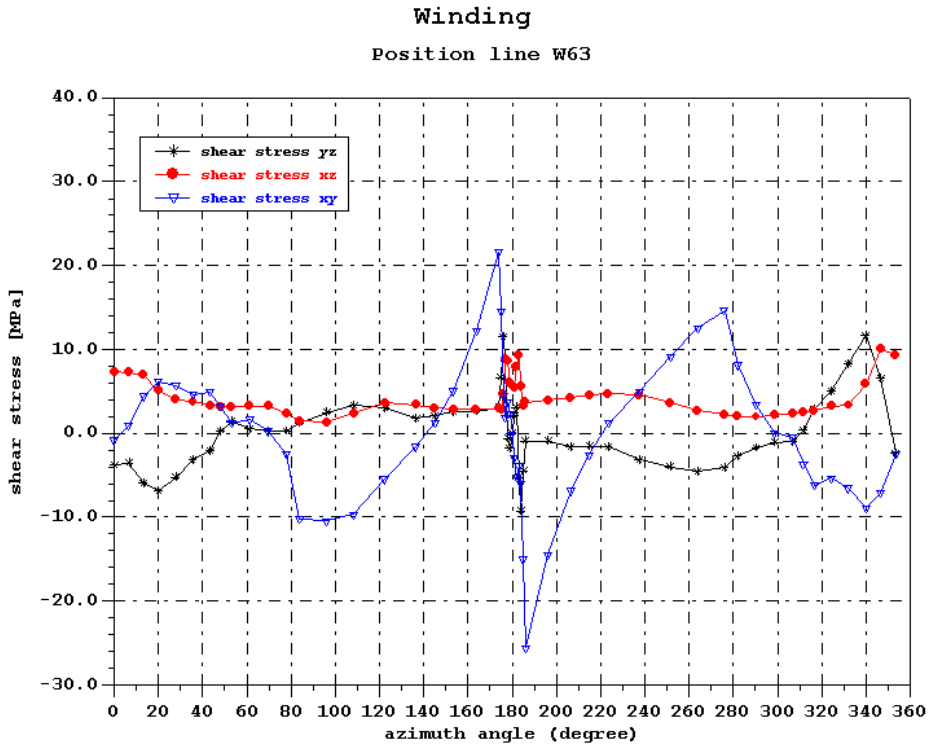

Legend: shear stress xz - τ_{rz}
shear stress yz - $\tau_{\varphi z}$
shear stress xy - $\tau_{r\varphi}$

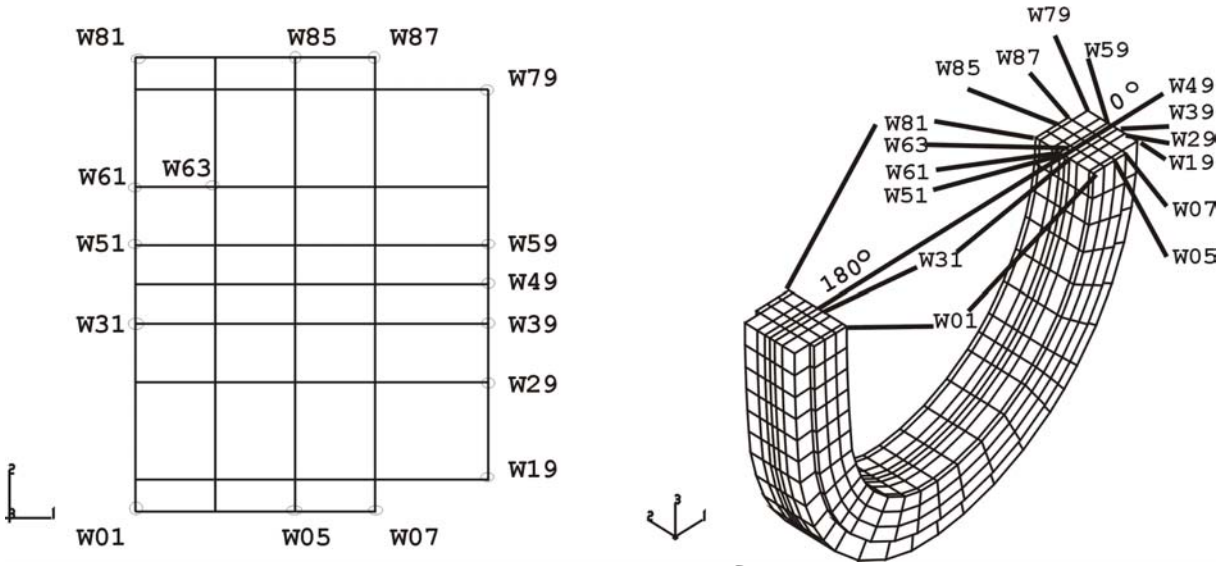

Figure 14 - Shear stresses of the LCT winding over the azimuth angle on the position line W63

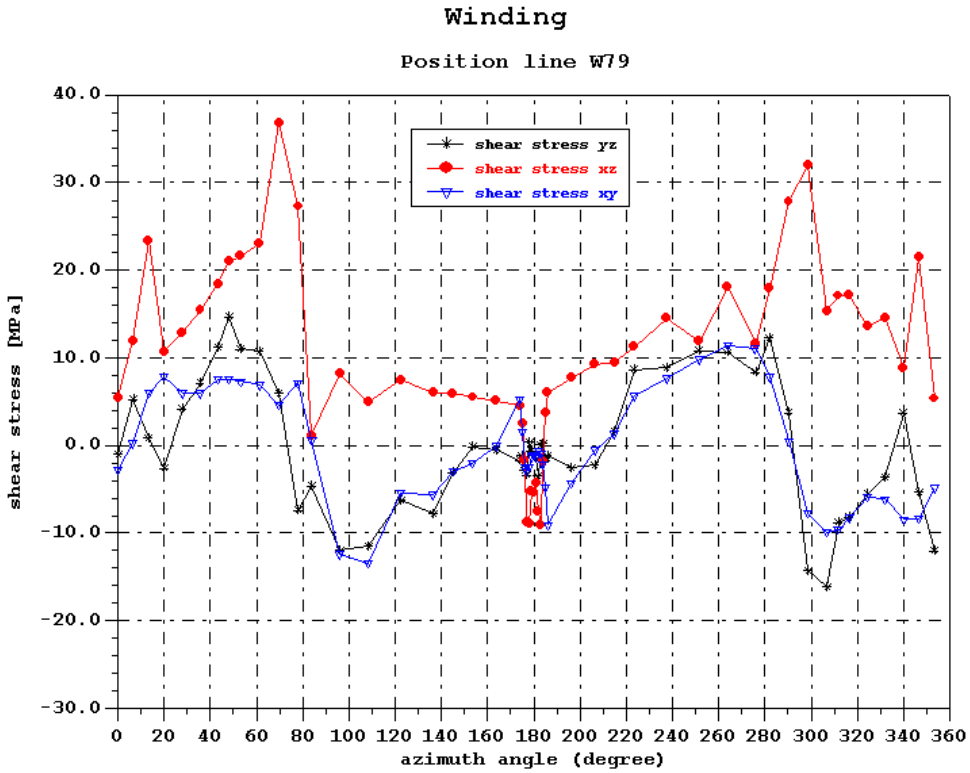

Legend: shear stress xz - τ_{rz}
shear stress yz - $\tau_{\varphi z}$
shear stress xy - $\tau_{r\varphi}$

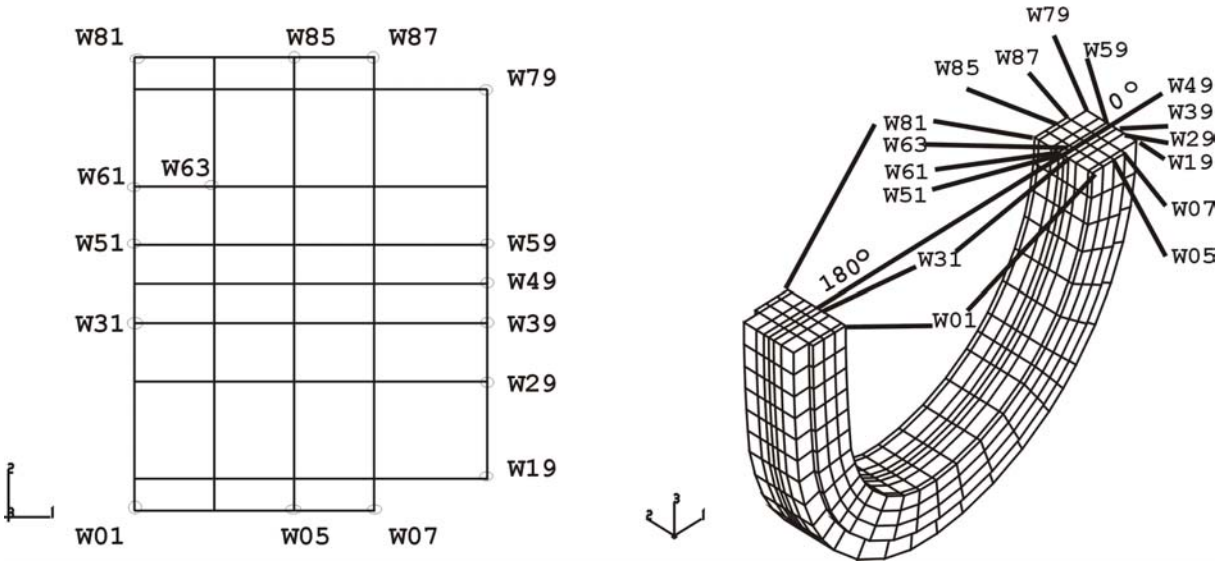

Figure 15 - Shear stresses of the LCT winding over the azimuth angle on the position line W79

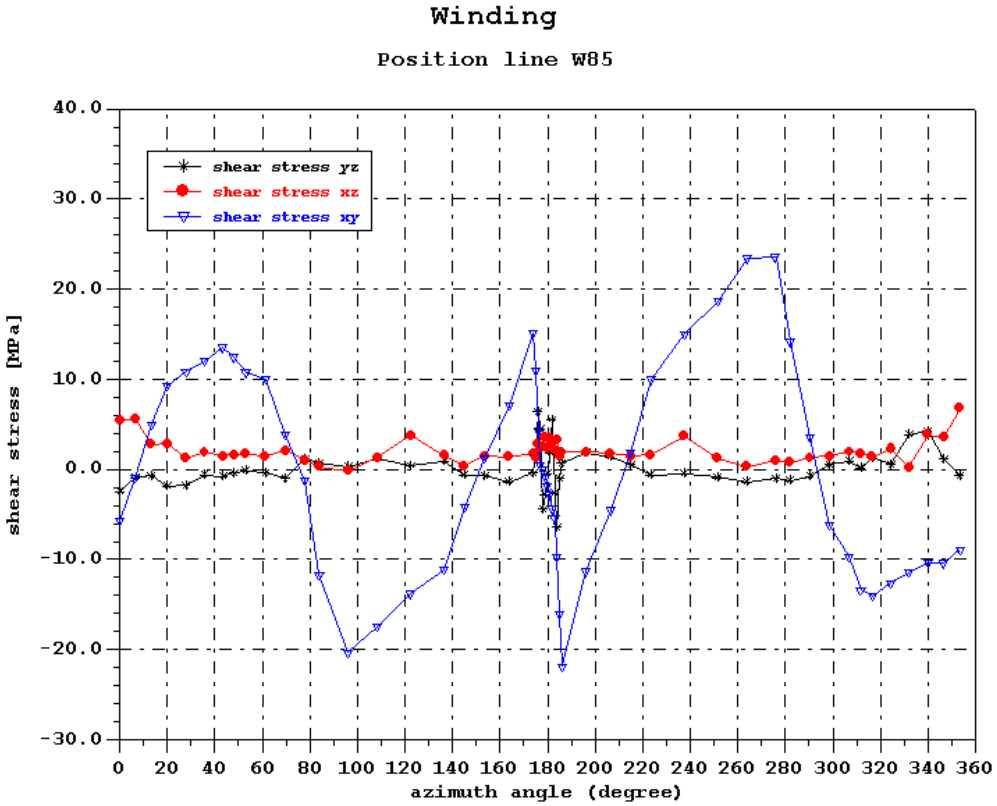

Legend: shear stress xz - τ_{rz}
shear stress yz - $\tau_{\varphi z}$
shear stress xy - $\tau_{r\varphi}$

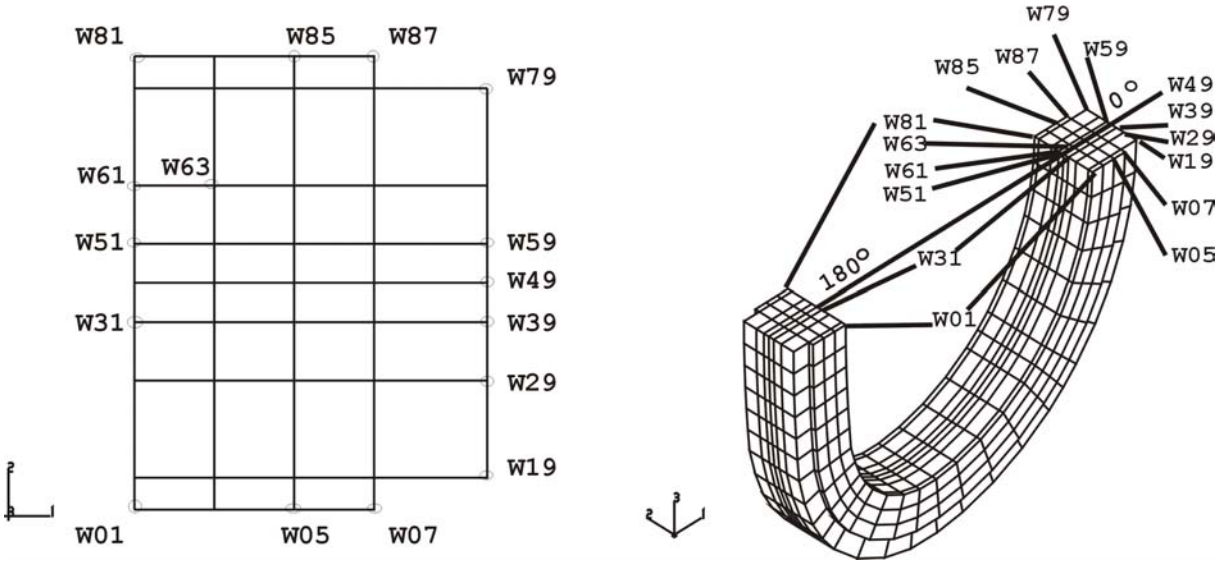

Figure 16 - Shear stresses of the LCT winding over the azimuth angle on the position line W85

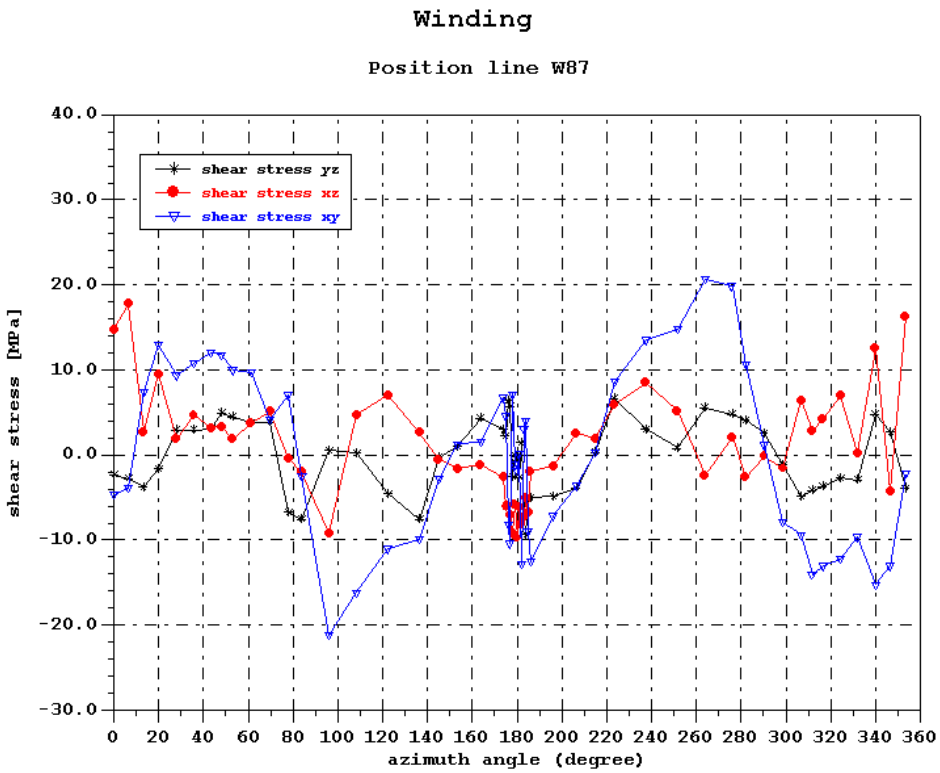

Legend: shear stress xz - τ_{rz}
shear stress yz - $\tau_{\varphi z}$
shear stress xy - $\tau_{r\varphi}$

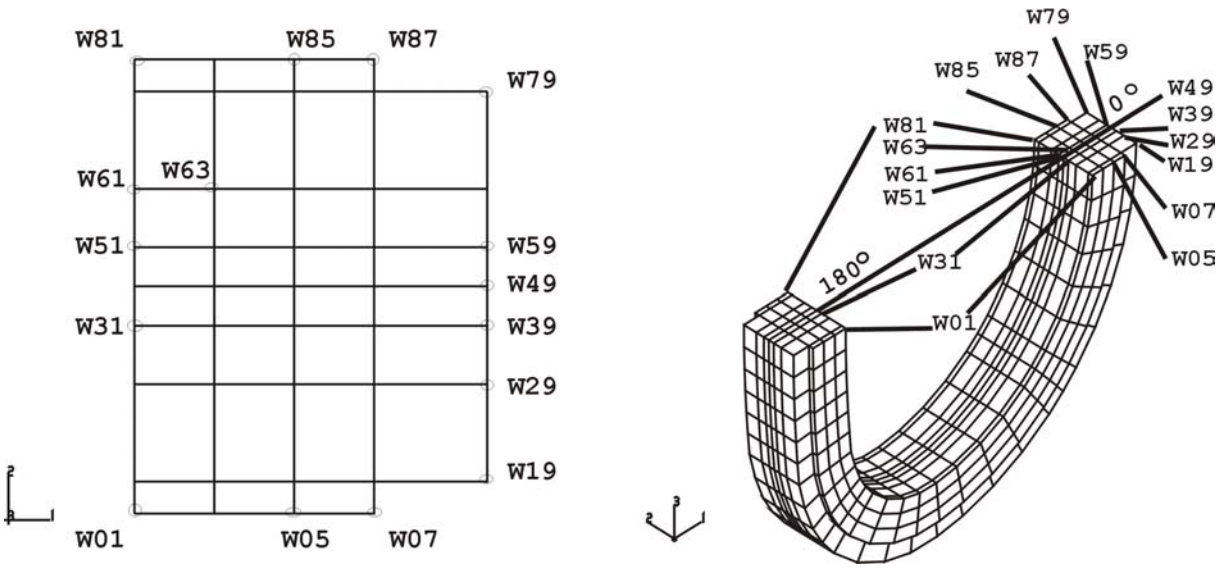

Figure 17 - Shear stresses of the LCT winding over the azimuth angle on the position line W87

The deformations of the casing are presented in figures 18, 19, 20 and 21 in top view, front view and side view, respectively.

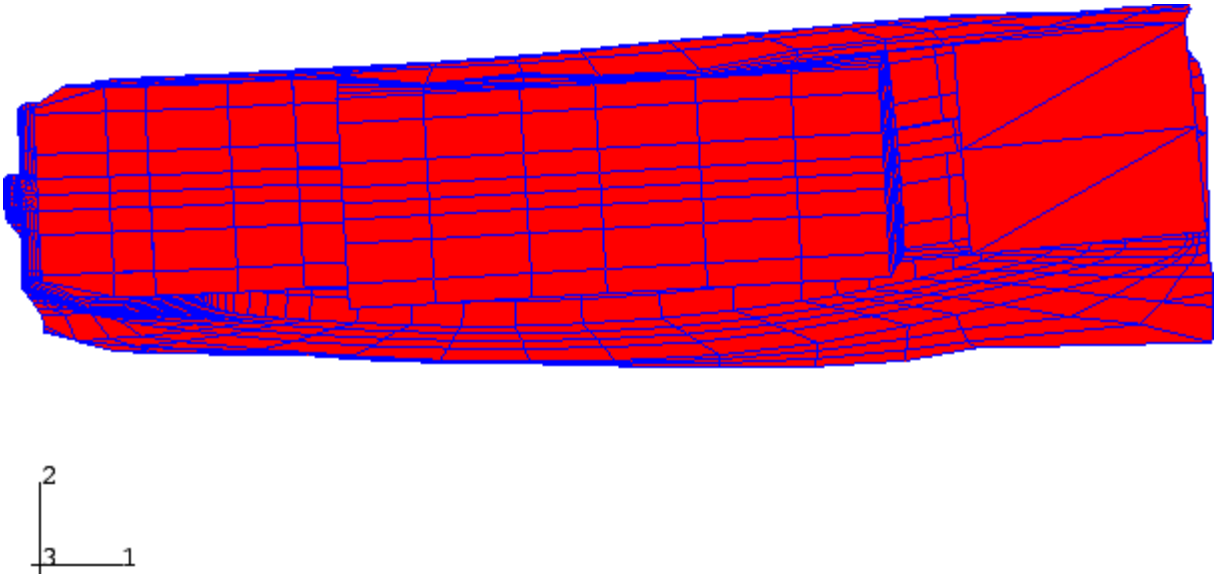

Figure 18 - Top view of the deformed LCT casing

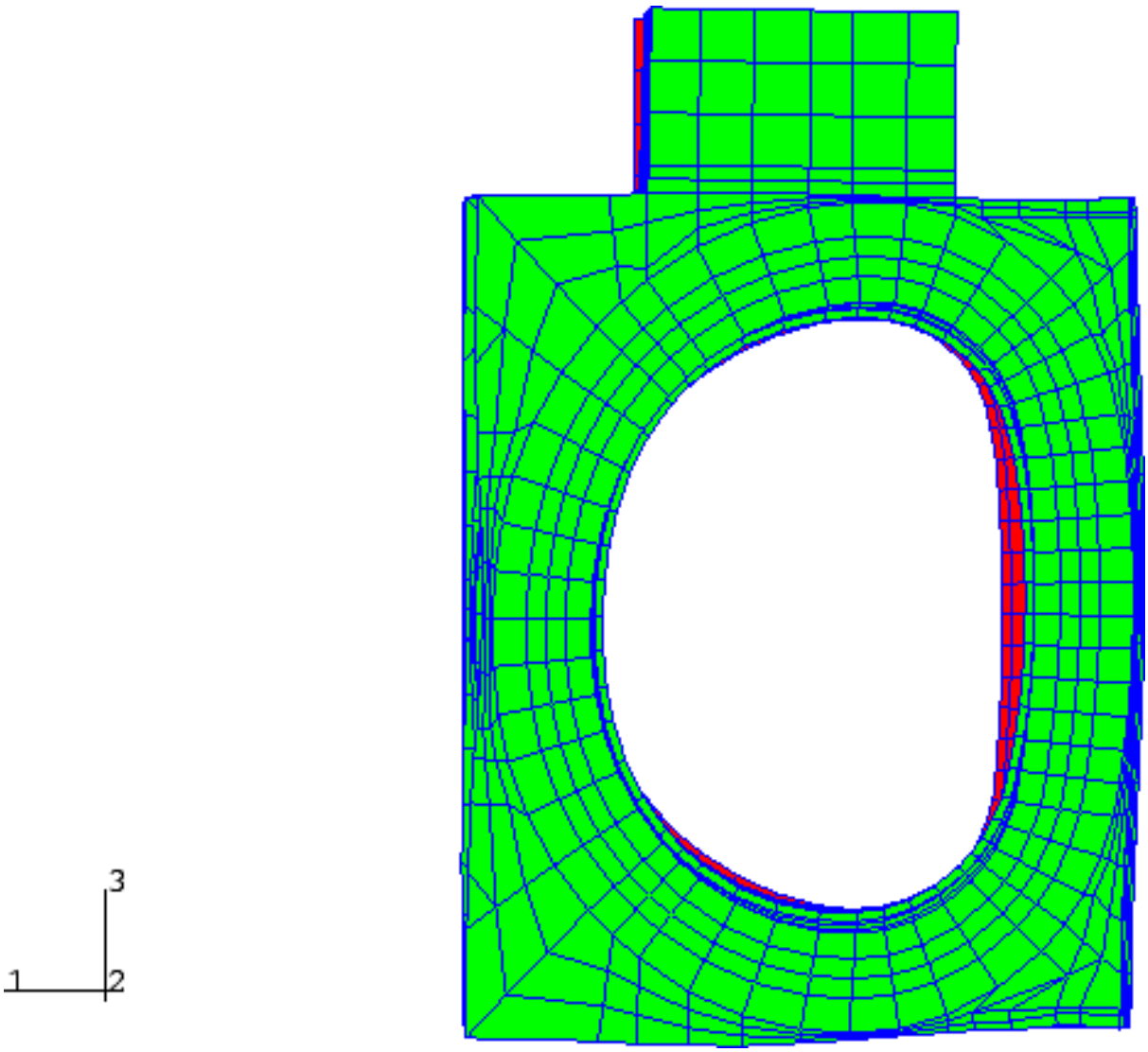

Figure 19 - Front view of the undeformed (red) and deformed (green) LCT casing

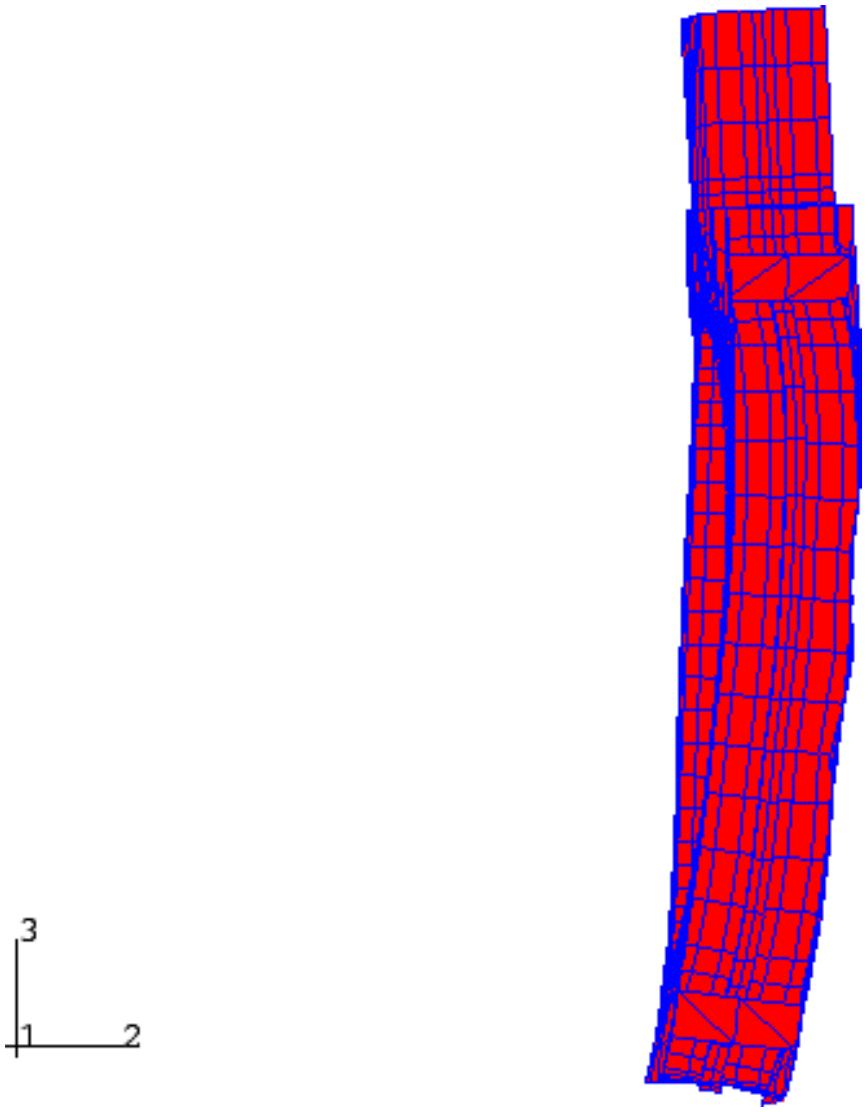

Figure 20 - Side view of the deformed LCT casing

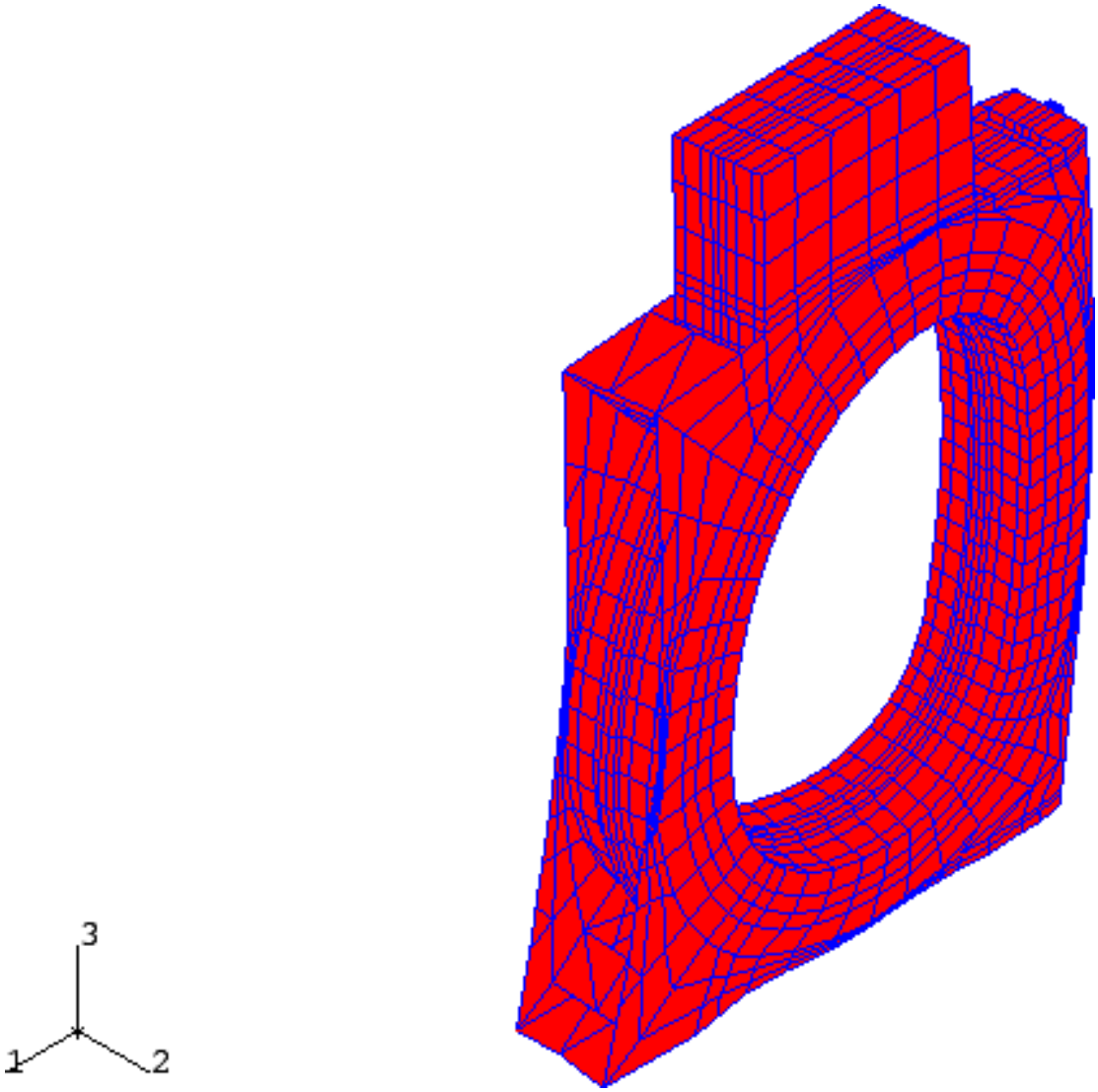

Figure 21 - Isometric view of the deformed LCT casing

In figure 22, the maximum displacements $\mathbf{u_x}$, $\mathbf{u_y}$, and $\mathbf{u_z}$ of the LCT casing are plotted over the azimuth angle of the casing. The maximum displacements are summarised in table 6. The $\mathbf{u_x}$ maximum displacement (-2.550 mm) occur at the inner edge of the side wall (position line G81), $\mathbf{u_z}$ (+1.292 mm) in the middle of the outer ring (position line G69) as well as (-2.260 mm) at the outer edge of the side wall (position line G89), and $\mathbf{u_y}$ (+9.072 mm) at the outer edge of the side wall (position line S85) of the LCT casing.

	displacement of the casing					
	u_x (mm)	**angle (^{o})**	**u_y (mm)**	**angle (^{o})**	**u_z (mm)**	**angle (^{o})**
max	**+0.250**	**316.50**	**+9.072**	**27.83**	**+1.292**	**78.00**
min	**-2.550**	**179.00**	**-1.391**	**298.67**	**-2.260**	**298.67**

Table 6

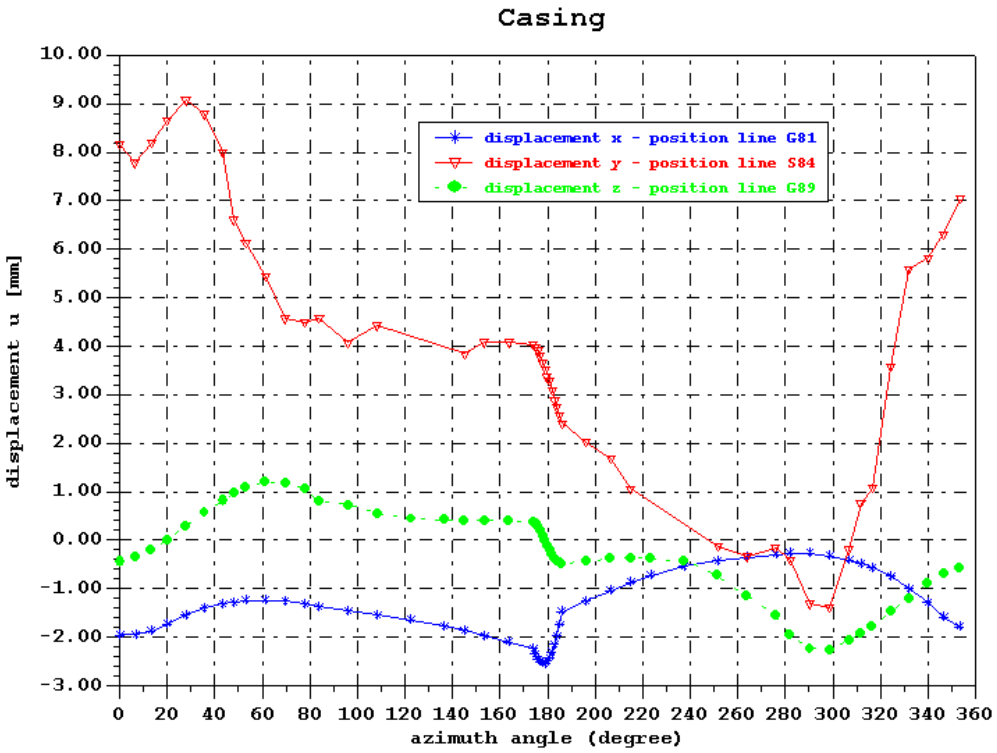

(figure legend: displacements x,y,z correspond to $\mathbf{u}_x$,$\mathbf{u}_y$,$\mathbf{u}_z$)

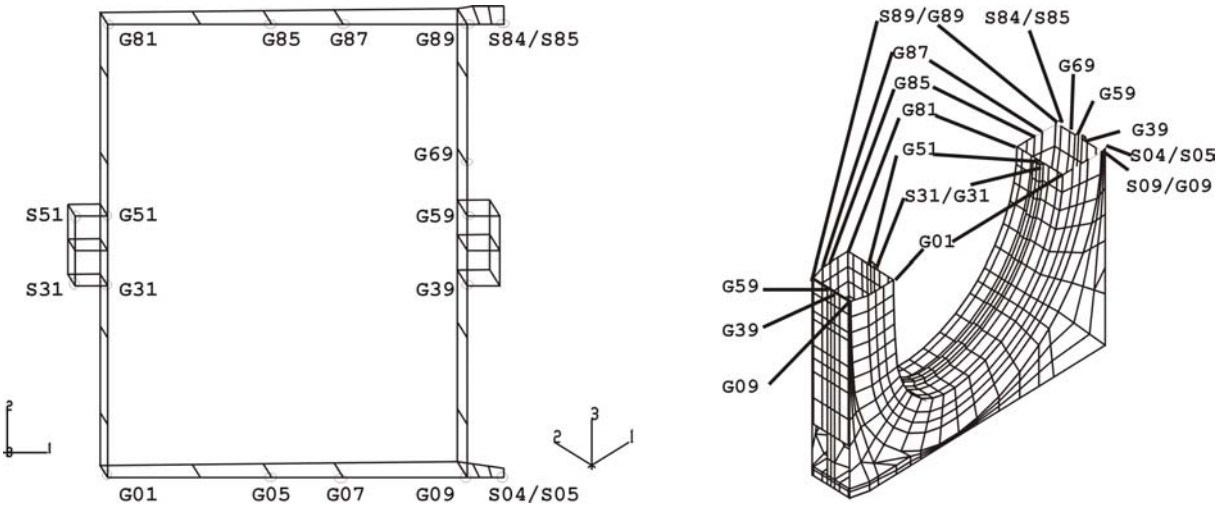

Figure 22 - Displacements of the LCT casing over the azimuth angle

As a result of the radial electromagnetic forces and the prescribed displacements, the LCT coil stretches in the middle of the inner ring (position line G41 – G41 is situated between G31 and G51) in x-direction at $\Delta x=0.422$ mm and reduces in z-direction at $\Delta z=0.300$ mm. The deformations are recognizable in figure 19. The prescribed displacements and the out-of-plane forces bend the LCT coil in y-direction (figures 18 and 20). The largest displacements are $ymax_1=9.072$ mm and $ymax_2=-1.391$ mm. All displacements of the LCT casing concerning the position lines G41, G81, S84, and G89 are summarized in tables 7, 8, 9 and 10.

Displacement of the LCT casing position line G81

node	angle (degree)	u_x (mm)	u_y (mm)	u_z (mm)
20081	0.0000	-1.9550	7.3760	-0.5774
20181	6.6667	-1.9460	7.5870	-0.3242
20281	13.3333	-1.8810	7.8560	-0.0798
20381	20.0000	-1.7250	7.9810	0.1856
20481	27.8333	-1.5500	8.0060	0.4448
20581	35.6667	-1.4060	7.9180	0.6900
20681	43.5000	-1.3110	7.7230	0.8717
20781	48.2500	-1.2860	7.5560	0.9749
20881	53.0000	-1.2500	7.3620	1.0430
20981	61.3333	-1.2500	6.9620	1.1090
21081	69.6667	-1.2550	6.5440	1.0830
21181	78.0000	-1.3200	6.1210	0.9588
21281	84.0000	-1.3760	5.8320	0.8440
21381	96.2500	-1.4580	5.5480	0.6764
21481	108.5000	-1.5450	5.3510	0.5518
21581	122.5000	-1.6420	5.1740	0.4105
21681	136.5000	-1.7790	5.0270	0.2942
21781	145.0000	-1.8670	4.9430	0.2359
21881	153.5000	-1.9730	4.8650	0.1820
21981	163.7500	-2.1010	4.7730	0.1281
22081	174.0000	-2.2320	4.6980	0.0867
22181	175.0000	-2.3540	4.5670	0.0484
22281	176.0000	-2.4590	4.4220	0.0226
22381	177.0000	-2.5120	4.3030	0.0037
22481	178.0000	-2.5380	4.1300	-0.0160
22581	179.0000	-2.5500	3.9650	-0.0177
22681	180.0000	-2.4880	3.8030	-0.0207
22781	181.0000	-2.4290	3.6480	-0.0199
22881	182.0000	-2.3060	3.4980	-0.0145
22981	183.0000	-2.1450	3.3700	-0.0160
23081	184.0000	-1.9760	3.2030	-0.0283
23181	185.0000	-1.7380	3.0620	-0.0283
23281	186.0000	-1.4740	2.9170	-0.0878
23381	196.2500	-1.2630	2.8000	-0.1101
23481	206.5000	-1.0390	2.6780	-0.1739
23581	215.0000	-0.8732	2.5730	-0.2303
23681	223.5000	-0.7244	2.4670	-0.3333
23781	237.5000	-0.5475	2.2880	-0.5397
23881	251.5000	-0.4240	2.1410	-0.8537
23981	263.7500	-0.3528	2.0720	-1.1540
24081	276.0000	-0.2930	2.1120	-1.4860
24181	282.0000	-0.2652	2.2940	-1.8060
24281	290.3333	-0.2640	2.6630	-2.0800
24381	298.6667	-0.3271	3.1480	-2.1570
24481	307.0000	-0.4113	3.7270	-2.1230
24581	311.7500	-0.4865	4.0750	-2.0430
24681	316.5000	-0.5663	4.4270	-1.9590
24781	324.3333	-0.7412	5.0180	-1.7790
24881	332.1667	-1.0030	5.5980	-1.5640
24981	340.0000	-1.2910	6.1680	-1.3230
25081	346.6667	-1.5940	6.6190	-1.0810
25181	353.3333	-1.7920	7.0320	-0.8385

Table 7

Displacement of the LCT casing position line S84

node	angle (degree)	u_x (mm)	u_y (mm)	u_z (mm)
30084	0.0000	-2.0850	8.1700	-0.4335
30184	6.6667	-2.1360	7.7760	-0.3264
30284	13.3333	-1.9570	8.1920	-0.2781
30384	20.0000	-1.6910	8.6560	-0.1645
30484	27.8333	-1.5240	9.0720	0.0685
30584	35.6667	-1.3090	8.7810	0.5921
30684	43.5000	-1.6820	8.0040	0.7892
30784	48.2500	-1.3630	6.6000	0.8466
30884	53.0000	-1.3290	6.1230	1.1650
30984	61.3333	-1.4010	5.4400	1.1770
31084	69.6667	-1.4260	4.5670	1.1300
31184	78.0000	-1.5030	4.4890	1.0180
31284	84.0000	-1.5500	4.5720	0.8390
31384	96.2500	-1.5950	4.0710	0.6892
31484	108.5000	-1.6230	4.4260	0.6260
31784	145.0000	-1.5530	3.8410	0.5090
31884	153.5000	-1.7040	4.0820	0.5200
31984	163.7500	-1.9010	4.0830	0.5041
32084	174.0000	-2.1190	4.0300	0.4287
32184	175.0000	-2.2260	3.9730	0.3697
32284	176.0000	-2.3110	3.9100	0.3057
32384	177.0000	-2.3890	3.8000	0.2277
32484	178.0000	-2.4420	3.6480	0.0917
32584	179.0000	-2.4200	3.5310	-0.0242
32684	180.0000	-2.3980	3.3630	-0.1084
32784	181.0000	-2.3250	3.2960	-0.1927
32884	182.0000	-2.2120	3.0930	-0.3010
32984	183.0000	-2.0130	2.8760	-0.4245
33084	184.0000	-1.8210	2.7420	-0.4940
33184	185.0000	-1.6280	2.5770	-0.5366
33284	186.0000	-1.4130	2.4070	-0.5711
33384	196.2500	-1.0580	2.0260	-0.5696
33484	206.5000	-0.7933	1.6830	-0.4930
33584	215.0000	-0.7365	1.0590	-0.1902
33884	251.5000	-0.8203	-0.1330	-0.7685
33984	263.7500	-0.8363	-0.3335	-1.1160
34084	276.0000	-0.7837	-0.1578	-1.5900
34184	282.0000	-0.6685	-0.4178	-1.9060
34284	290.3333	-0.4905	-1.3120	-2.2410
34384	298.6667	-0.2682	-1.3910	-2.1850
34484	307.0000	-0.1470	-0.1985	-2.0210
34584	311.7500	-0.1647	0.7688	-1.7290
34684	316.5000	-0.3172	1.0830	-1.3710
34784	324.3333	-0.3729	3.5700	-1.2480
34884	332.1667	-0.8625	5.5880	-0.8235
34984	340.0000	-1.1300	5.8220	-0.6420
35084	346.6667	-1.5070	6.3090	-0.5269
35184	353.3333	-1.9080	7.0420	-0.5368

Table 8

Displacement of the LCT casing position line G89

node	angle (degree)	u_x (mm)	u_y (mm)	u_z (mm)
20089	0.0000	-2.0560	7.6460	-0.4476
20189	6.6667	-2.1180	8.0130	-0.3422
20289	13.3333	-1.9610	7.8830	-0.2080
20389	20.0000	-1.6540	8.6280	0.0010
20489	27.8333	-1.4210	8.6360	0.2888
20589	35.6667	-1.3590	8.4160	0.5601
20689	43.5000	-1.2730	7.9520	0.8146
20789	48.2500	-1.3220	7.4750	0.9834
20889	53.0000	-1.2720	6.9350	1.0770
20989	61.3333	-1.3230	6.2840	1.2110
21089	69.6667	-1.3750	5.0300	1.1740
21189	78.0000	-1.4530	4.6380	1.0600
21289	84.0000	-1.5480	4.8070	0.8056
21389	96.2500	-1.5880	4.1300	0.7224
21489	108.5000	-1.6180	4.6250	0.5513
21589	122.5000	-1.6000	4.1870	0.4443
21689	136.5000	-1.6470	4.3650	0.4184
21789	145.0000	-1.7290	4.3150	0.4064
21889	153.5000	-1.7900	4.2470	0.4050
21989	163.7500	-1.9490	4.1880	0.4059
22089	174.0000	-2.1090	4.1090	0.3804
22189	175.0000	-2.2320	4.0360	0.3362
22289	176.0000	-2.3370	3.9260	0.2739
22389	177.0000	-2.4080	3.8330	0.1892
22489	178.0000	-2.4510	3.7080	0.0909
22589	179.0000	-2.4210	3.5550	-0.0057
22689	180.0000	-2.4050	3.4290	-0.1040
22789	181.0000	-2.3080	3.2740	-0.1987
22889	182.0000	-2.2190	3.1380	-0.2865
22989	183.0000	-2.0660	2.9880	-0.3694
23089	184.0000	-1.8710	2.7910	-0.4375
23189	185.0000	-1.6290	2.6100	-0.4648
23289	186.0000	-1.3860	2.3830	-0.4875
23389	196.2500	-1.1220	2.0890	-0.4372
23489	206.5000	-0.8913	1.7660	-0.3861
23589	215.0000	-0.7178	1.5270	-0.3620
23689	223.5000	-0.6088	1.2530	-0.3886
23789	237.5000	-0.6033	0.4426	-0.4276
23889	251.5000	-0.6869	0.3486	-0.7307
23989	263.7500	-0.7790	-0.2002	-1.1490
24089	276.0000	-0.7292	0.0380	-1.5640
24189	282.0000	-0.5661	-0.0860	-1.9450
24289	290.3333	-0.3876	-0.0549	-2.2390
24389	298.6667	-0.3811	0.6224	-2.2600
24489	307.0000	-0.3753	2.4010	-2.0630
24589	311.7500	-0.3903	2.8880	-1.9120
24689	316.5000	-0.3994	3.5060	-1.7700
24789	324.3333	-0.5522	4.4460	-1.4760
24889	332.1667	-0.7434	5.1880	-1.2050
24989	340.0000	-1.1010	6.0010	-0.8862
25089	346.6667	-1.5700	5.7310	-0.7015
25189	353.3333	-1.9270	7.1670	-0.5876

Table 9

Displacement of the LCT casing position line G41

node	angle (degree)	u_x (mm)	u_y (mm)	u_z (mm)
20041	0.0000	-2.0790	7.3870	-0.0722
20141	6.6667	-2.0620	7.6720	-0.0475
20241	13.3333	-1.9000	7.8840	0.0065
20341	20.0000	-1.6350	8.0130	0.1097
20441	27.8333	-1.2990	8.0380	0.2842
20541	35.6667	-1.0110	7.9370	0.4849
20641	43.5000	-0.8111	7.7250	0.6686
20741	48.2500	-0.7430	7.5510	0.7527
20841	53.0000	-0.7233	7.3480	0.7921
20941	61.3333	-0.7597	6.9460	0.7598
21041	69.6667	-0.8485	6.5200	0.6020
21141	78.0000	-0.9452	6.1010	0.3139
21241	84.0000	-0.9908	5.8170	0.0543
21341	96.2500	-0.9883	5.5500	-0.1915
21441	108.5000	-0.9520	5.3630	-0.3046
21541	122.5000	-0.9367	5.1900	-0.3037
21641	136.5000	-1.0020	5.0450	-0.2024
21741	145.0000	-1.0980	4.9630	-0.1116
21841	153.5000	-1.2490	4.8850	-0.0135
21941	163.7500	-1.4800	4.7930	0.0810
22041	174.0000	-1.7320	4.7030	0.1303
22141	175.0000	-2.0250	4.5720	0.1783
22241	176.0000	-2.2540	4.4320	0.1926
22341	177.0000	-2.4090	4.2810	0.2017
22441	178.0000	-2.4950	4.1210	0.2087
22541	179.0000	-2.5240	3.9590	0.2146
22641	180.0000	-2.5010	3.7980	0.2192
22741	181.0000	-2.4310	3.6420	0.2231
22841	182.0000	-2.3080	3.4920	0.2273
22941	183.0000	-2.1190	3.3470	0.2329
23041	184.0000	-1.8450	3.2040	0.2423
23141	185.0000	-1.4810	3.0630	0.2625
23241	186.0000	-1.0570	2.9250	0.2981
23341	196.2500	-0.7384	2.8120	0.3966
23441	206.5000	-0.4685	2.7000	0.5093
23541	215.0000	-0.3091	2.5990	0.6169
23641	223.5000	-0.2289	2.4910	0.7009
23741	237.5000	-0.2216	2.3100	0.7414
23841	251.5000	-0.3017	2.1550	0.6174
23941	263.7500	-0.3735	2.0840	0.3531
24041	276.0000	-0.3792	2.1140	-0.0180
24141	282.0000	-0.3056	2.2730	-0.4997
24241	290.3333	-0.1724	2.6200	-0.9283
24341	298.6667	-0.0668	3.1070	-1.1390
24441	307.0000	-0.0465	3.6920	-1.1630
24541	311.7500	-0.0891	4.0490	-1.1010
24641	316.5000	-0.1901	4.4150	-0.9886
24741	324.3333	-0.4551	5.0230	-0.7584
24841	332.1667	-0.8236	5.6190	-0.5136
24941	340.0000	-1.2610	6.1900	-0.2992
25041	346.6667	-1.6350	6.6370	-0.1700
25141	353.3333	-1.9240	7.0420	-0.1014

Table 10

In figures 23, 24, and 25, the displacement distributions of the LCT casing, u_x, u_y, and u_z are plotted in discrete filled colour levels in a detail of the structure. Each coloured contour corresponds to a range bounded by the values indicated on the similarly coloured band within the legend.

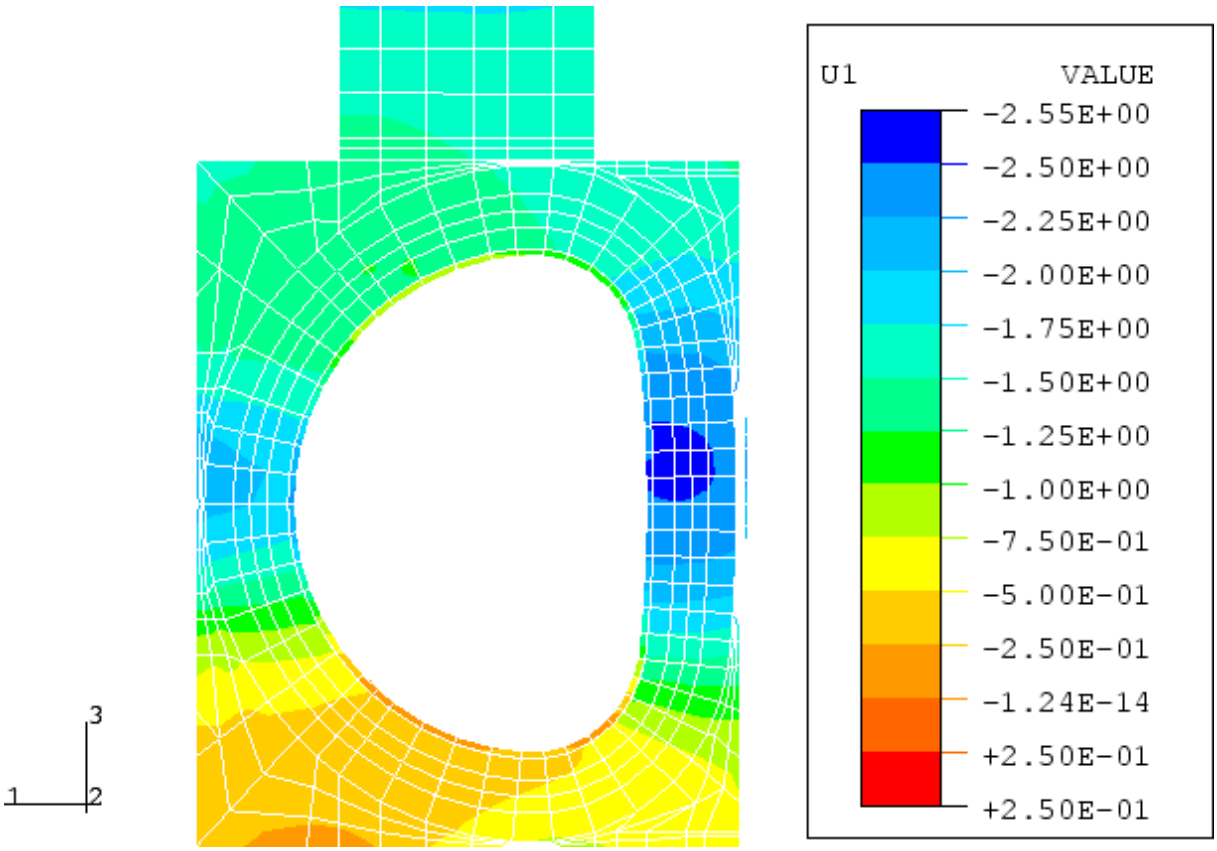

Figure 23 - Contour plot of the displacement u_x of the LCT casing

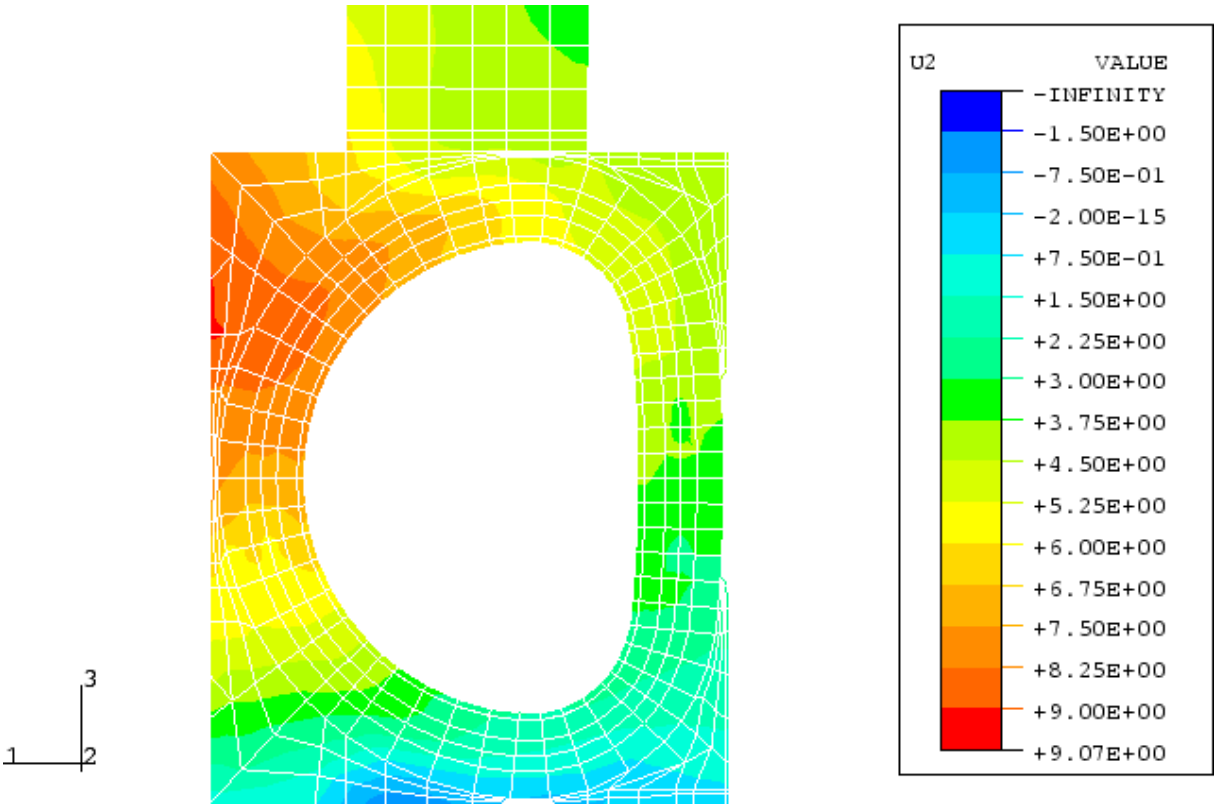

Figure 24 - Contour plot of the displacement u_y of the LCT casing

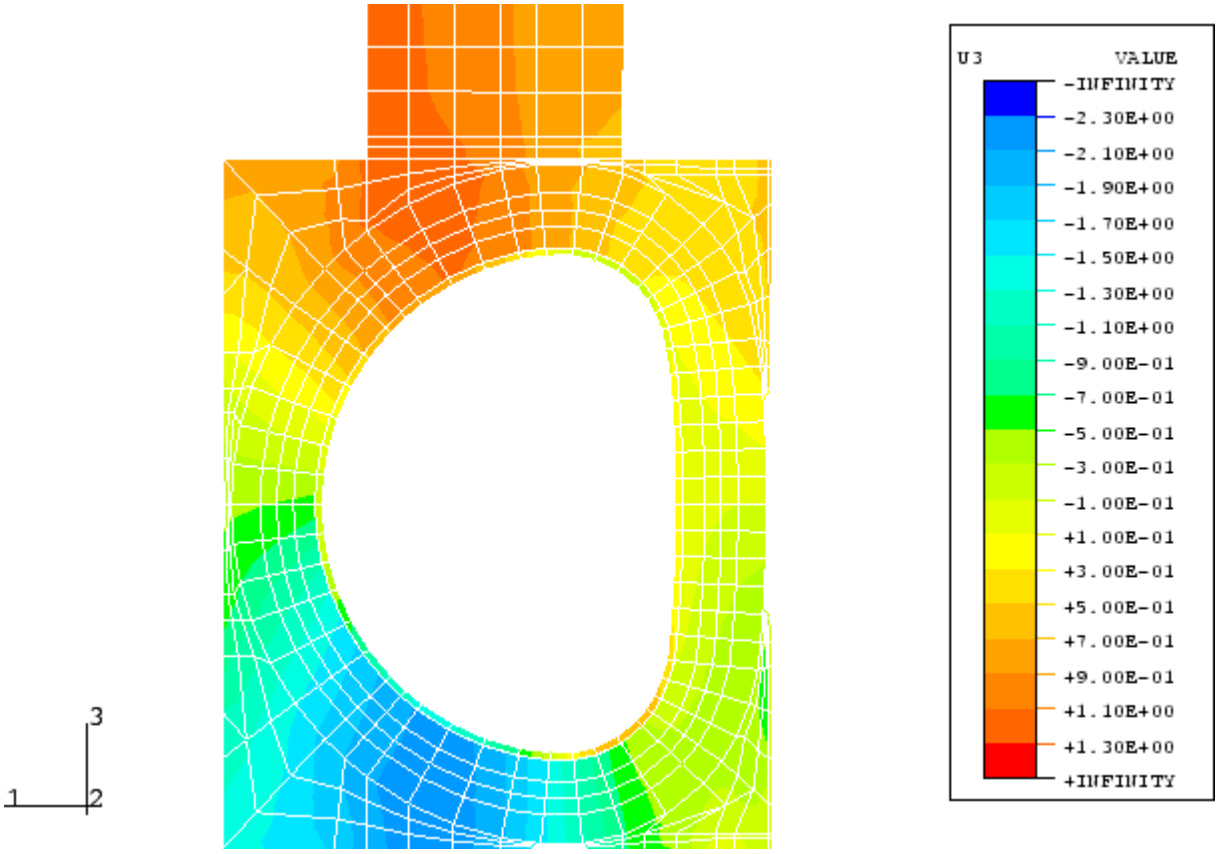

Figure 25 - Contour plot of the displacement u_z of the LCT casing

The deformations of the winding are plotted in figures 26, 27, 28, and 29 in the top view, front view, and side view, respectively.

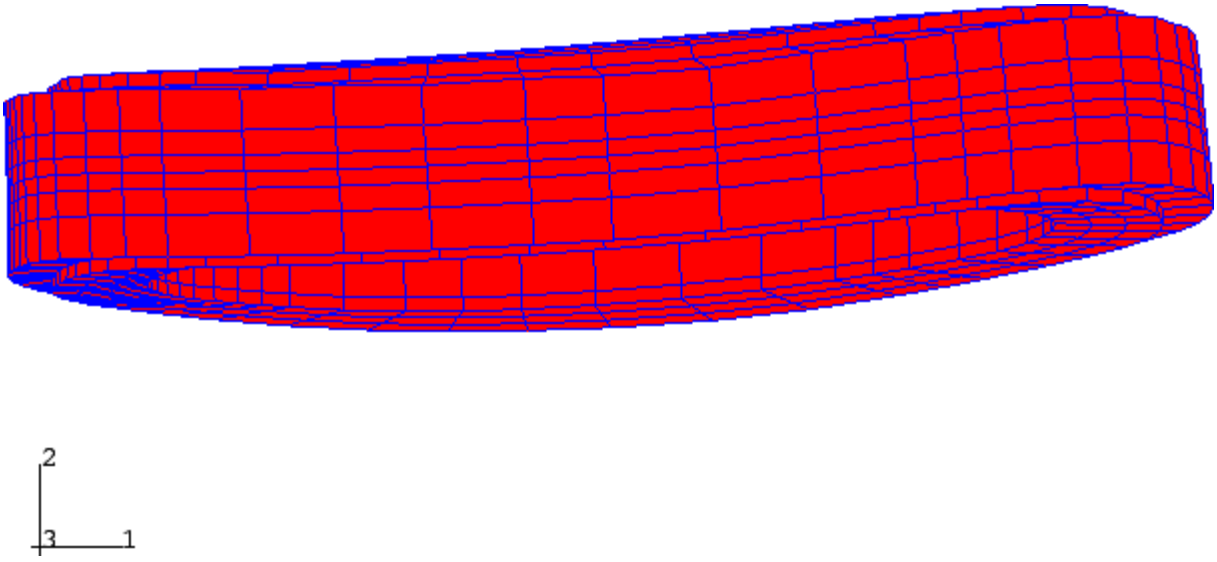

Figure 26 - Top view of the deformed LCT winding

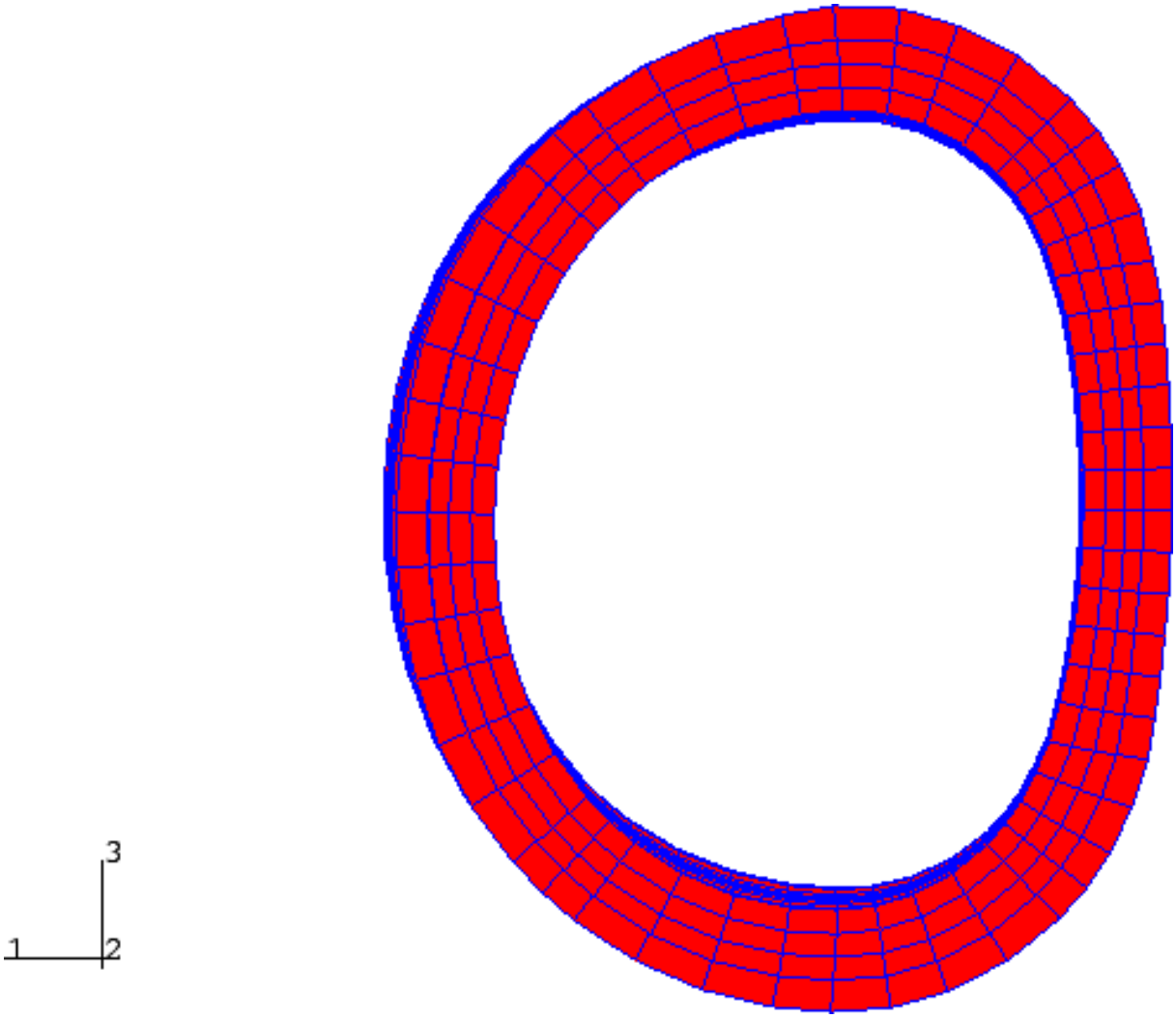

Figure 27 - Front view of the deformed LCT winding

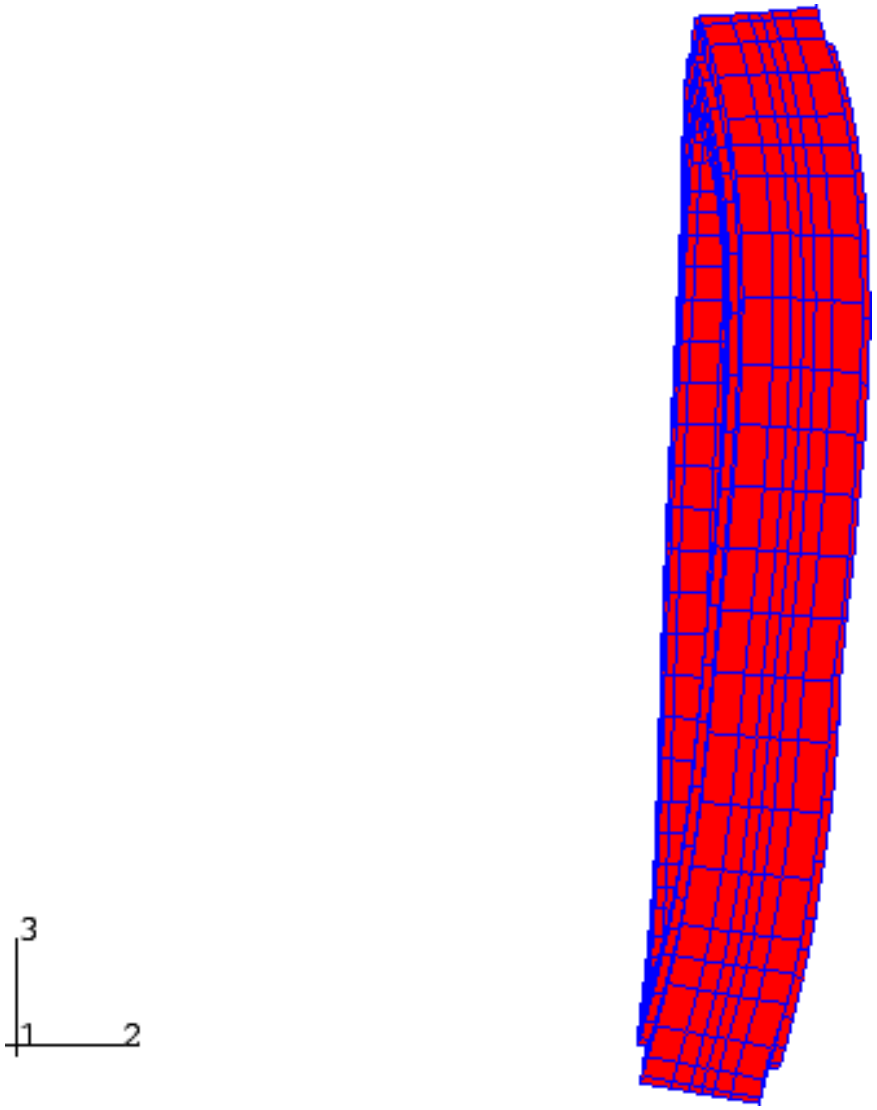

Figure 28 - Side view of the deformed LCT winding

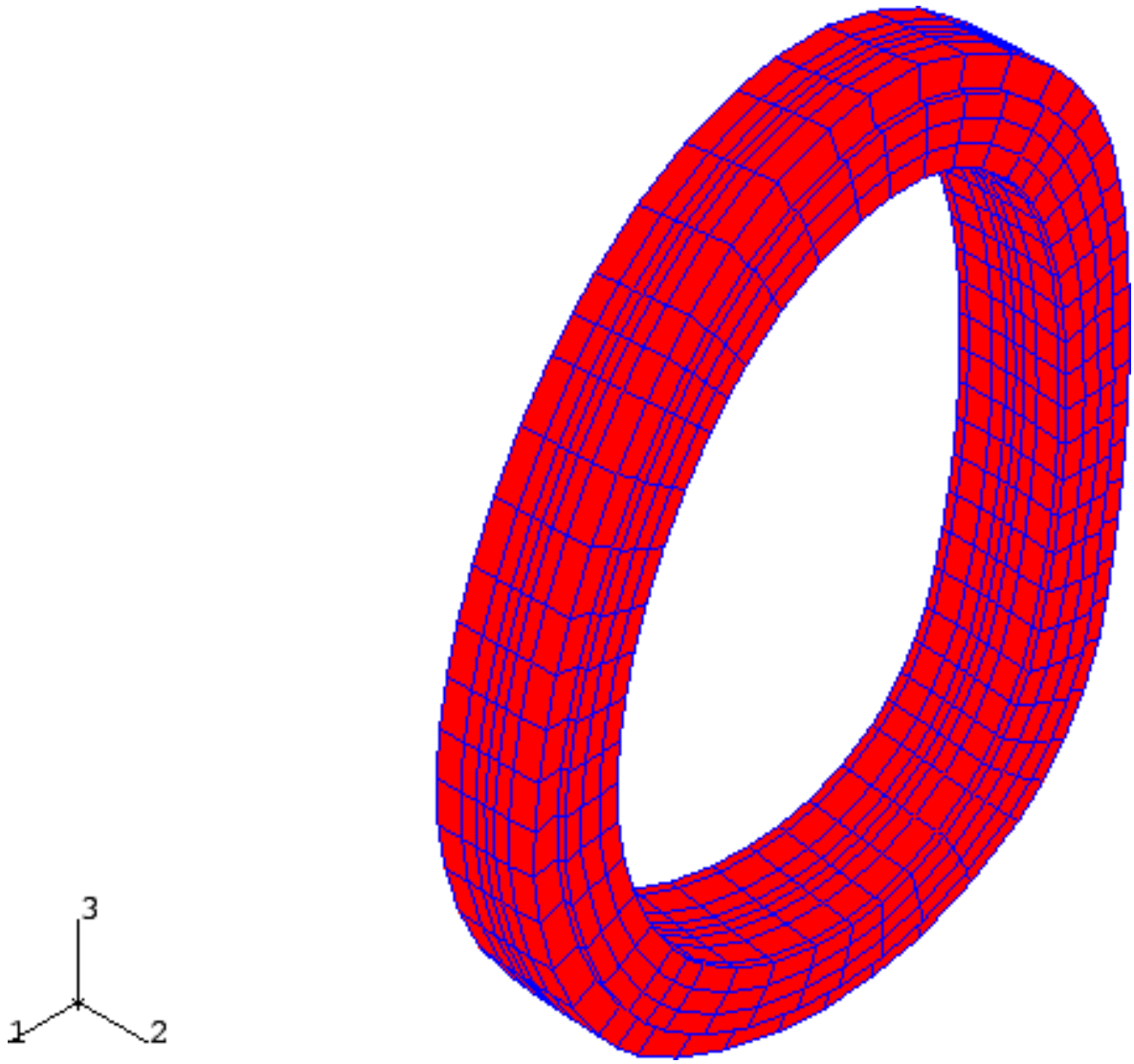

Figure 29 - Isometric view of the deformed LCT winding

The maximum displacement $\mathbf{u_x}$ occurs in the middle of the inner ring (position line W51), $\mathbf{u_z}$ on the border of the inner ring (position line W81), and $\mathbf{u_y}$ in the middle of the outer ring (position line W29) of the LCT winding. In figure 30, $\mathbf{u_x}$, $\mathbf{u_y}$, and $\mathbf{u_z}$ of the LCT winding are plotted over the azimuth angle of the winding. The maximum displacements are summarised in table 11.

	displacement of the winding					
	u_x (mm)	**angle (^{o})**	**u_y (mm)**	**angle (^{o})**	**u_z (mm)**	**angle (^{o})**
max	**+0.804**	**311.75**	**+8.893**	**27.83**	**+1.844**	**69.67**
min	**-4.218**	**180.00**	**+0.182**	**263.75**	**-2.552**	**298.67**

Table 11

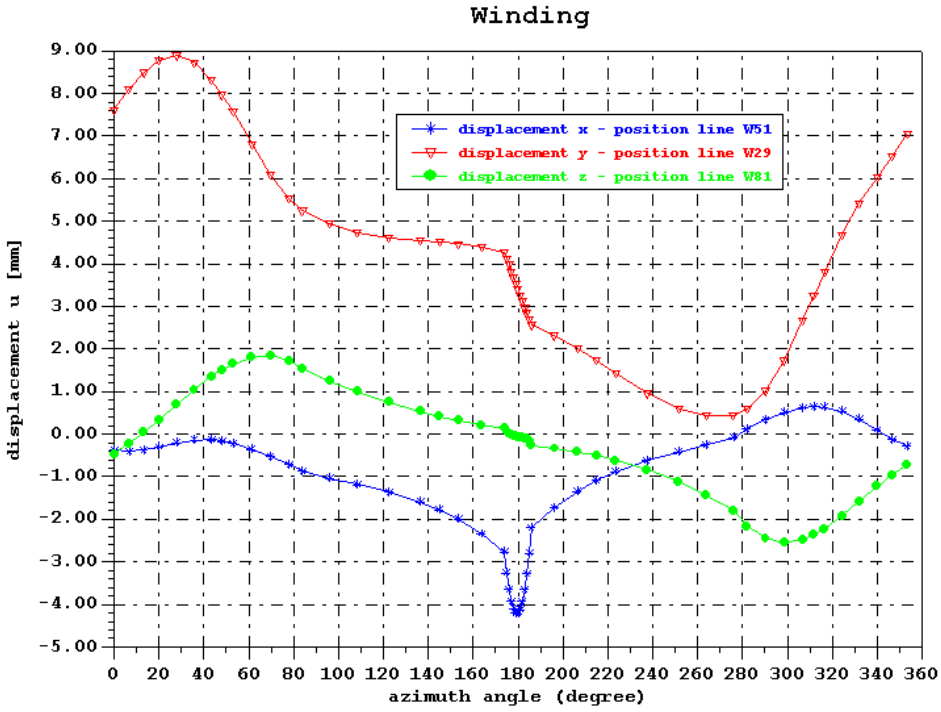

(figure legend: displacements x,y,z correspond to $\mathbf{u}_x$,$\mathbf{u}_y$,$\mathbf{u}_z$)

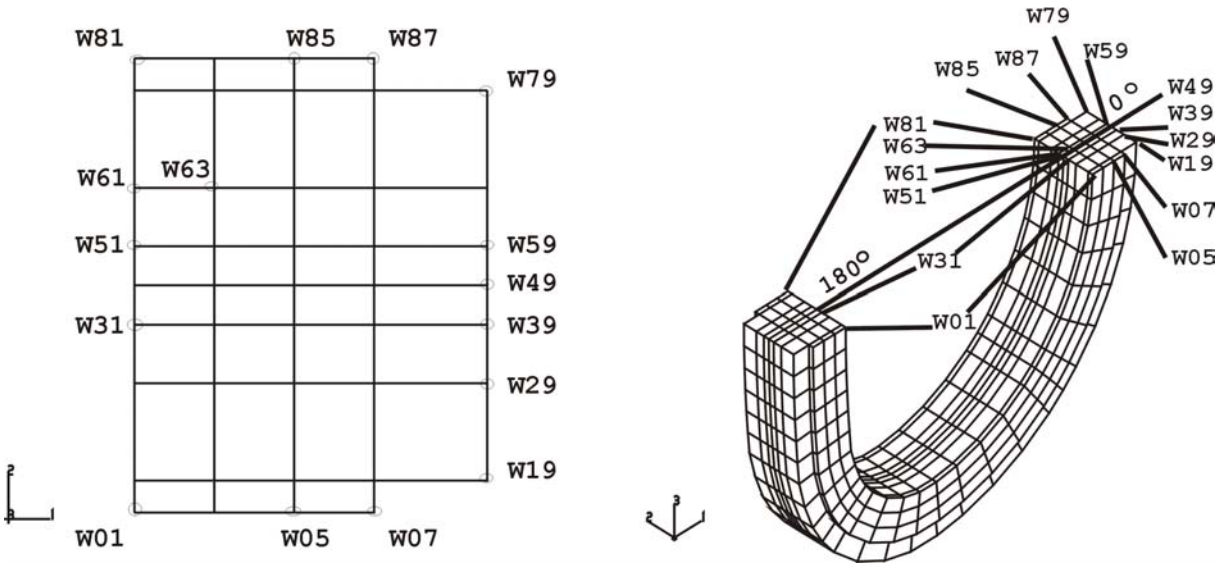

Figure 30 - Displacements of the LCT winding over the azimuth angle

3. Conclusion

For the test configuration consisting of the LCT coil, the intercoil structure, and the ITER-TF model coil, the estimate with the assumed boundary conditions shows that the stresses in the LCT winding and casing are not critical.

4. References

/1/ - S.J. Sackett, UCID 176221 “EFFI – a code for calculating the electromagnetic field, force and inductance in coil systems of arbitary geometry”, 1977
/2/ - ABAQUS USER MANUAL, Version 5.8, Hibbitt, Karlson & Sorensen, Inc.
/3/ - A. Grünhagen, unpublished report Kernforschungszentrum Karlsruhe, Oktober 1992
/4/ - ABAQUS/Post Reference Guide Version 5.8, Hibbitt, Karlson & Sorensen, Inc.
/5/ - S. Raff, unpublished report
/6/ - ABAQUS/Viewer Reference Guide Version 6.2, Hibbitt, Karlson & Sorensen, Inc.